UiT
THE ARCTIC
UNIVERSITY
OF NORWAY

Faculty of Science and Technology
Department of Geosciences

Use of 2D-seismic data and available wells to investigate the source potential of the Palaeozoic interval in the Loppa High area, SW Barents Sea

—

Asbjørn Hetland

Master thesis in Geology [GEO-3900]
May 2018

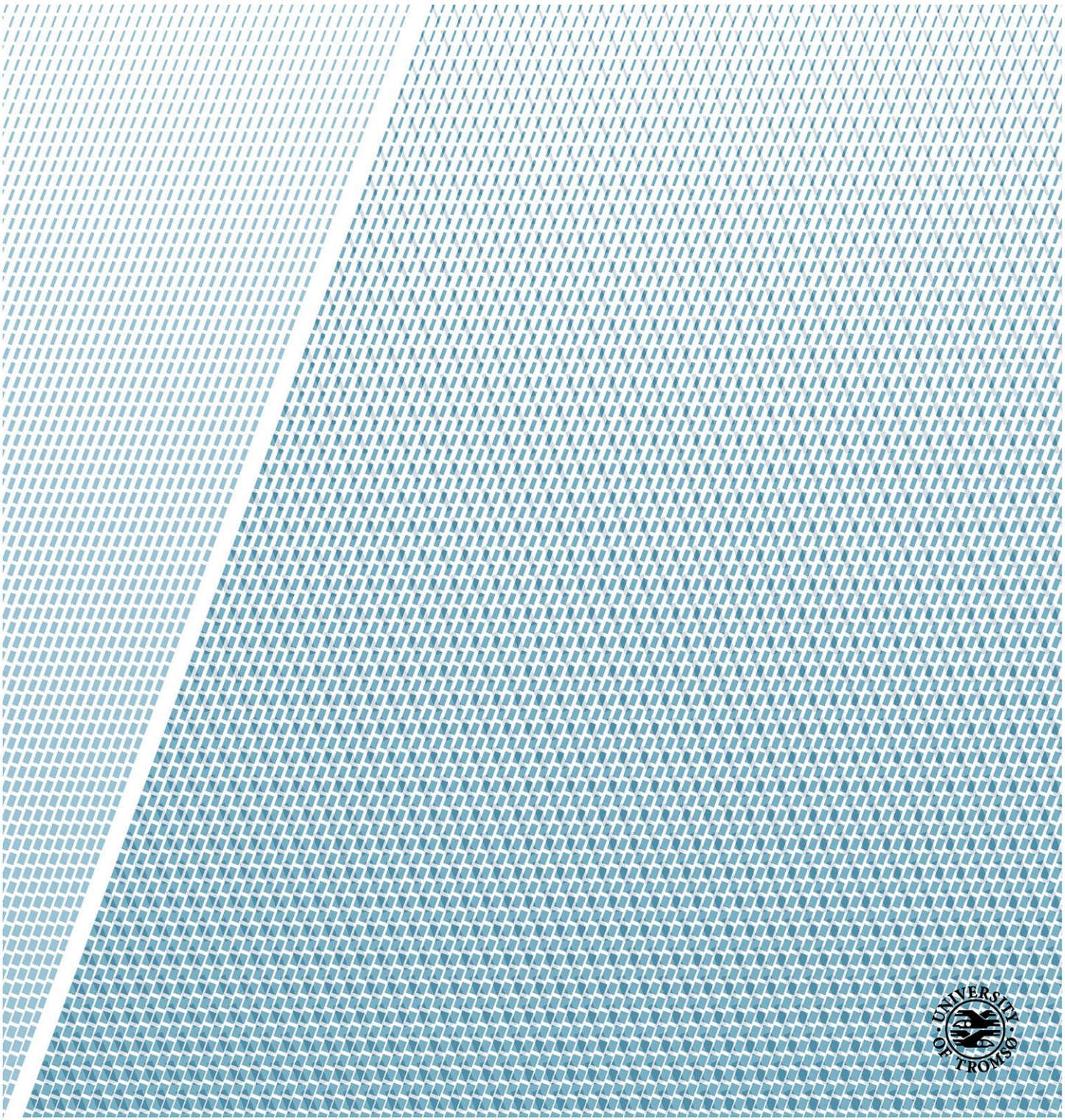

Abstract

While most established plays in the Barents Sea have occurred in the Mesozoic, the Alta and Gohta discoveries prove a new carbonate play concept, with a source rock that does not stem from the Jurassic. Based on depositional environment and TOC values from the Palaeozoic interval a source rock with Top Ørn as its bottom and Top Røye as its top was interpreted. Basin modelling carried out on this potential source rock concludes that the Palaeozoic interval in the Loppa High area have a good source potential. A total of 30 different models have been carried out and three highlighted models, the P10, P50 and P90 model all shows evidence of good maturity ranges (ranging from 0.5 %R_o to 1.5 %R_o) and generation potential.

Acknowledgement

I have to thank my supervisors, Iver Martens and Tom Arne Rydningen, they have given my every opportunity to write a good thesis and I appreciate all the help I've received.

Thank you, Martin, Lars & Sebbi for making the hours spent in the office a treat, and you're also pretty decent room mates!

Thank you to my family for your encouraging words in times of need, and last but not least, thank you Helle for your love and support throughout my studies.

-

Asbjørn Hetland

Tromsø

Table of Contents

1 Objectives & Introduction

1.1 Objectives

The Loppa High area (Fig. 1.1) has experienced an increased interest from the oil industry following the major Gotha (7120/1-3) and Alta (7220/11-1) discoveries, which proved commercial volumes of oil in carbonates of Permian age.

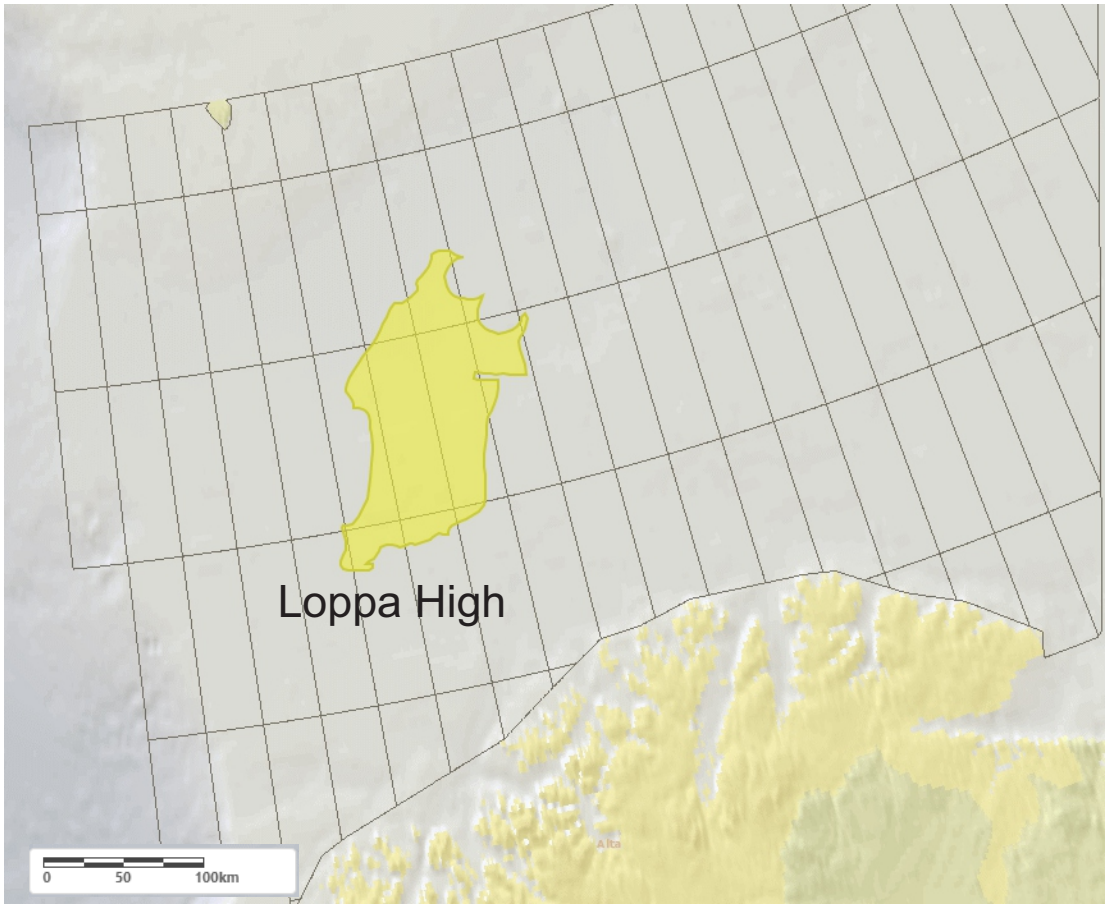

Fig. 1.1 Overview over the Loppa High placement in the Barents Sea.

The information regarding the Carboniferous and Permian plays is sparse and the companies with information in this area are keeping their cards tight to their chests. Critical factors in the plays are mentioned to be both source rock distribution and reservoir quality.

The overall goal of the project is to investigate and model the hydrocarbon generation potential of Permian and Carboniferous source rocks in the Loppa High area. Through investigation of petrophysical and geochemical properties from available well data a quick look basin modelling study will be performed.

The thesis will use available 2D seismic lines and public available wells that have penetrated formations of Permian and Carboniferous age.

1.2 The Barents Sea

The Barents Sea, named after the Dutch explorer Willem Barents, spans an area of 1.4 million km^2, with an average depth of ~300m, which makes it one of the largest areas of continental shelf on earth. The Barents Sea (Fig. 1.2) is bracketed by the Norwegian and Russian mainland to the south, the Norwegian Sea to the west, Svalbard to the north-west, Franz Josef Land to the northeast and Novaya Zemlya to the east (Doré, 1994).

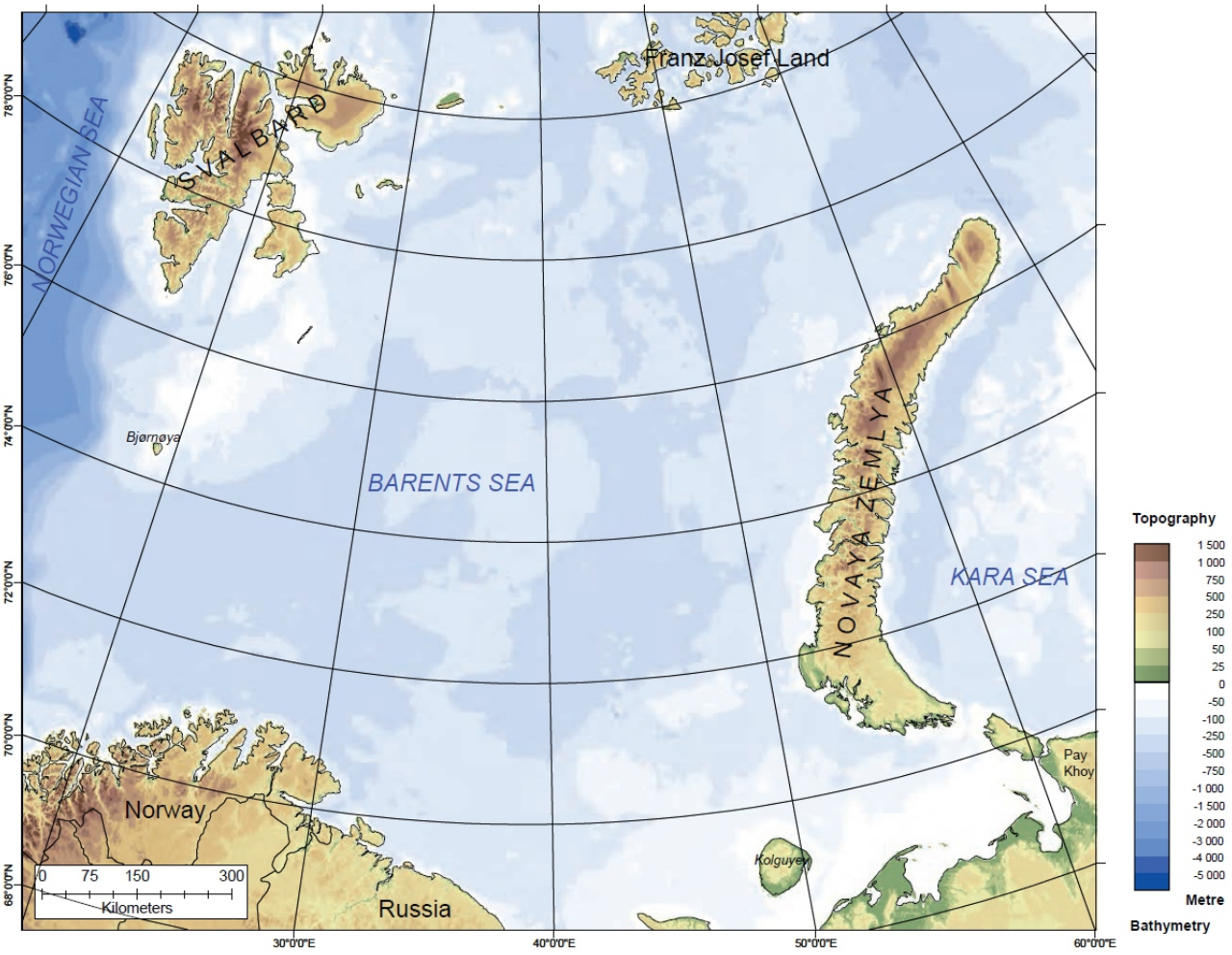

Fig. 1.2 Map showing the Barents Sea with the adjacent landmasses bracketing the ocean. (Figure from Smelror et al., 2009.)

In the 1970s, Norway started with hydrocarbon exploration in the Barents Sea, but only through seismic and aero-magnetic surveys. It was not until 1980 the first exploration well (7119/12-1) was spudded – 1 year after the government gave “the green light” for arctic drilling. Since then there have been drilled over 130 wells on the Norwegian side of the Barents Sea.

In the early 1980s, several gas discoveries were made – Askeladd in 1981, Albatross in 1982 and Snøhvit in 1984. After this great start the optimism were high and several wells were drilled in the years to come, but after 1986 the wells contained only small gas resources or were completely dry. As a result no wells were drilled between 1994 and 2000.

When drilling resumed in year 2000 the optimism again came with it. The first part of the Goliat field were discovered in 2000 and in 2006 two more discoveries made the field commercial. It continued with Skrugard and Havis (now Johan Castberg) in 2011 and 2012, Wisting and Gohta in 2013 and Alta in 2014.

The biggest field on the Norwegian side of the Barents Sea is the Snøhvit field, it is estimated to contain 224 billion Sm^3 recoverable gas (NPD, 2017c). This is a fairly big field, but the arctic have proven to contain even bigger fields – On the Russian side of the Barents Sea we find the Shtokmanovskoye field, which holds estimated gas-resources of 3200 billion m^3 (NPD, 2004). So the Barents Sea is still highly interesting for future exploration, it has proven to contain several hydrocarbon fields, and the Norwegian Petroleum Directorate estimates that the Barents Sea contains 1.4 billion Sm^3 undiscovered resources (NPD, 2017d).

1.3 Petroleum exploration at Loppa High

The first hydrocarbon discovery within the Loppa High area was made in 1989, this was a non-commercial discovery and never received an official name (today it is know as "7120/1-2") (Fig. 1.3).

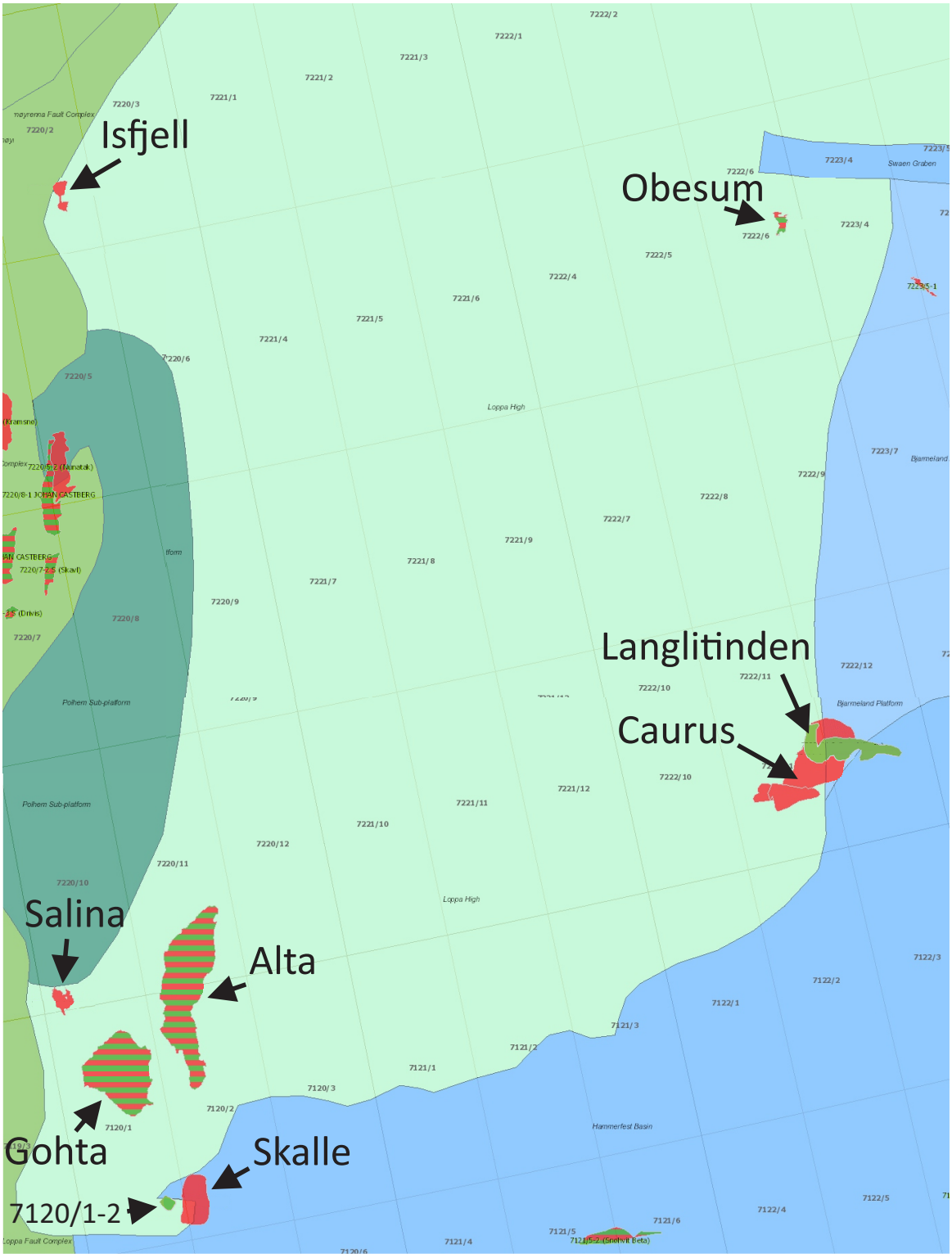

Fig. 1.3 Loppa high (light green) with all its corresponding discoveries.

After the first discovery it took almost 20 years before a new discovery was made, which was the oil/gas field “Obesum”, a discovery by Statoil in 2008. Obesum also proved to be non-commercial, but the area had again proven that hydrocarbons were present.
For the years to come several discoveries were made (Table 1.1), including the Gohta and Alta discoveries. These two discoveries are estimated to contain 350 million barrels of oil, and will likely be further developed and end up as producing fields.

Table 1.1 All petroleum discoveries made within the Loppa High boundary

Name	Year	Well	Company	Content
7120/1-2	1989	7120/1-2	Lundin Norway AS	Oil
Obesum	2008	7222/6-1 S	Statoil Petroleum AS	Oil/Gas
Caurus	2008	7222/11-1	Statoil Petroleum AS	Oil/Gas
Skalle	2011	7120/2-3 S	Lundin Norway AS	Gas
Salina	2012	7220/10-1	Eni Norge AS	Gas
Gohta	2013	7120/1-3	Lundin Norway AS	Oil/Gas
Langlitinden	2014	7222/11-2	Det norske oljeselskap ASA	Oil
Alta	2014	7220/11-1	Lundin Norway AS	Oil/Gas
Isfjell	2014	7220/2-1	Statoil Petroleum AS	Gas

1.3.1 Plays and petroleum systems

A petroleum system is a term describing a system that have all the prerequisite in order to generate and store oil. The prerequisites processes are trap formation, generation, migration and accumulation and the prerequisite elements are source, reservoir, seal and overburden rock. All the mentioned processes must be placed in time and space in a order such that the processes required to form a petroleum accumulation can occur (Dow, 1994).

According to NPD (NPD, 2017a) the Loppa High area is affected by three different plays (Table 1.2). They define a play as "a geographically and stratigraphically delimited area where a specific set of geological factors such as reservoir rock, trap, mature source rock and migrations paths exist in order that petroleum may be provable."

Table 1.2 Plays and petroleum systems in Loppa High (NPD, 2017a).

	Lower Carboniferous	Carboniferous to Permian	Middle to Upper Permian
Reservoir	Sandstone and conglomerates from Billefjorden GP.	Limestone and dolomites from Gipsdalen GP.	Limestone and dolomites from Tempelfjorden GP.
Depositional Environment	Fluvial and alluvial, floodplain and river deposits.	Carbonate build-ups in shallow marine, warm water.	Marine, temperate water.
Trap	Structural and stratigraphic.	Thought to be stratigraphic, but might also be a combination of stratigraphic and structural.	Stratigraphic, but also contains a combination of stratigraphic and structural.
Source Rock	Upper Devonian – Lower Carboniferous coal and carbonaceous shales from Billefjorden GP.	Lower Carboniferous coal from Billefjorden GP and Upper Permian shales from Tempelfjorden GP.	Lower Carboniferous coal from Billefjorden GP, Upper Permian shales from Tempelfjorden GP and Middle Triassic shales from Steinkobbe FM.
Description	This play is currently categorized as “unconfirmed”, meaning the only evidence is the oil shows from well 7120/2-1. The critical factors are preservation and leakage owed to tilting, reactivation of faults and Cenozoic uplift and erosion, especially for areas with shallow and/or truncated structures.	This play is proven in Loppa High through the Alta discovery (well 7220/11-1). The critical factors are the presence of a mature source rock, the reservoir quality and the fact that the area has been affected by tilting, reactivation of faults and Cenozoic uplift and erosion.	This play is proven in Loppa High through the Gohta discovery (well 7120/1-3). The critical factors are presence of reservoir and the reservoir quality. This area has also been affected by tilting, reactivation of faults and Cenozoic uplift and erosion.

1.4 Source rock

A source rock refers to a rock that have generated or has the potential to generate hydrocarbons. The key elements in a source rock is its organic content (created by burial in anoxic environments) and the temperature it has been exposed to (burial history).

A source rock is classified after which Kerogen type it is. There are four different types of Kerogen and they are distinguished based on depositional environment and from what organism/plant the organic content derives from. The kerogen type tells us more about what type of hydrocarbon we can expect to see if the source rock in fact have generated hydrocarbons, and together with vitrinite reflectance one can determine if the source has hit the oil/gas-window (Fig. 1.4).

Kerogen type I

• Predominantly from lacustrine environments (marine in some cases).

• Derived from algae and plankton.

• Rich in hydrogen and low in oxygen.

• Oil prone.

Kerogen type II

• Typically generated in reducing marine environments.

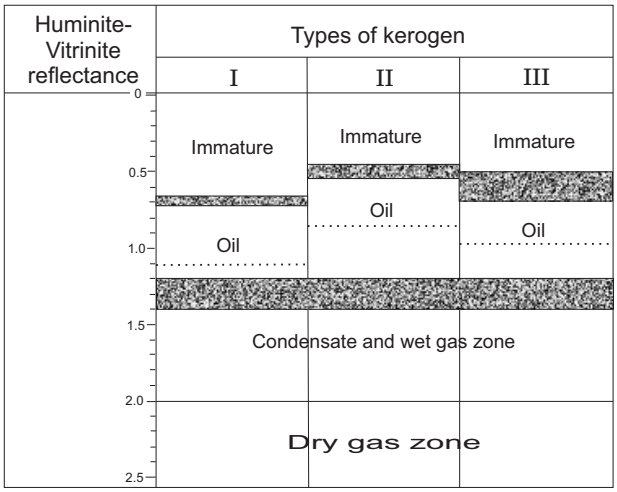

Fig. 1.4 Approximate boundaries of the gas and oil zones in terms of vitrinite reflectance. (Stippled line is peak oil generation.) (Figure from Tissot, 1984).

• Derived mainly from plankton.

• Rich in hydrogen and low in carbon and oxygen.

• Oil prone.

Kerogen type III

• Mainly shallow to deep marine or non marine environments.

• Derived primarily from terrigenous plant debris.

• Low hydrogen and high oxygen content.

• Tends to generate dry gas.

Kerogen type IV

• Derived from residual organic matter that have been reworked.

• High carbon and oxygen content and poor in hydrogen.

• No potential for generating oil and gas.

(Jacobson, 1991)

The depositional environment in the Loppa High area around Permian times will result in a Kerogen type II, which is the one represented in the Røye FM.

1.4.1 Palaeozoic source rock in SW Barents Sea

Røye FM is a interesting formation in terms of source rock potential. Its upper lithology consist of silicified calcareous claystone with minor pyrite and traces of organic material, in the lower part of the formation it is characterised by silty carbonate mudstone, interbedded silicified marls and calcareous claystone with some thin bed of spiculitic cherts (Larssen et al., 2002). The age of Røye FM was in 1994 suggested to be of Kungurian (283-272 Mya) to Kazanian age (270-260 Mya), based on cores from 7128/12-U-01 and 7129/10-U-01 (Mangerud, 1994; Bugge et al., 1995). The organic materials encountered in this formation is what makes it interesting in terms of source potential, in well 7128/6-1 upper Permian marine limestones were encountered, cores containing these limestones (Fig. 1.5), showed a interval with TOC ranging from 1.4 to 2.0 wt% (Pedersen et al., 2006). A study made by Ohm et al. in 2008 on TOC values in the Barents Sea (Fig. 1.6) suggests Upper Permian TOC values to range from 0.7% to 3.5%.

Fig. 1.5 Upper Permian marine limestone of the Røye FM from well 7128/6-1. (NPD, 2017b)

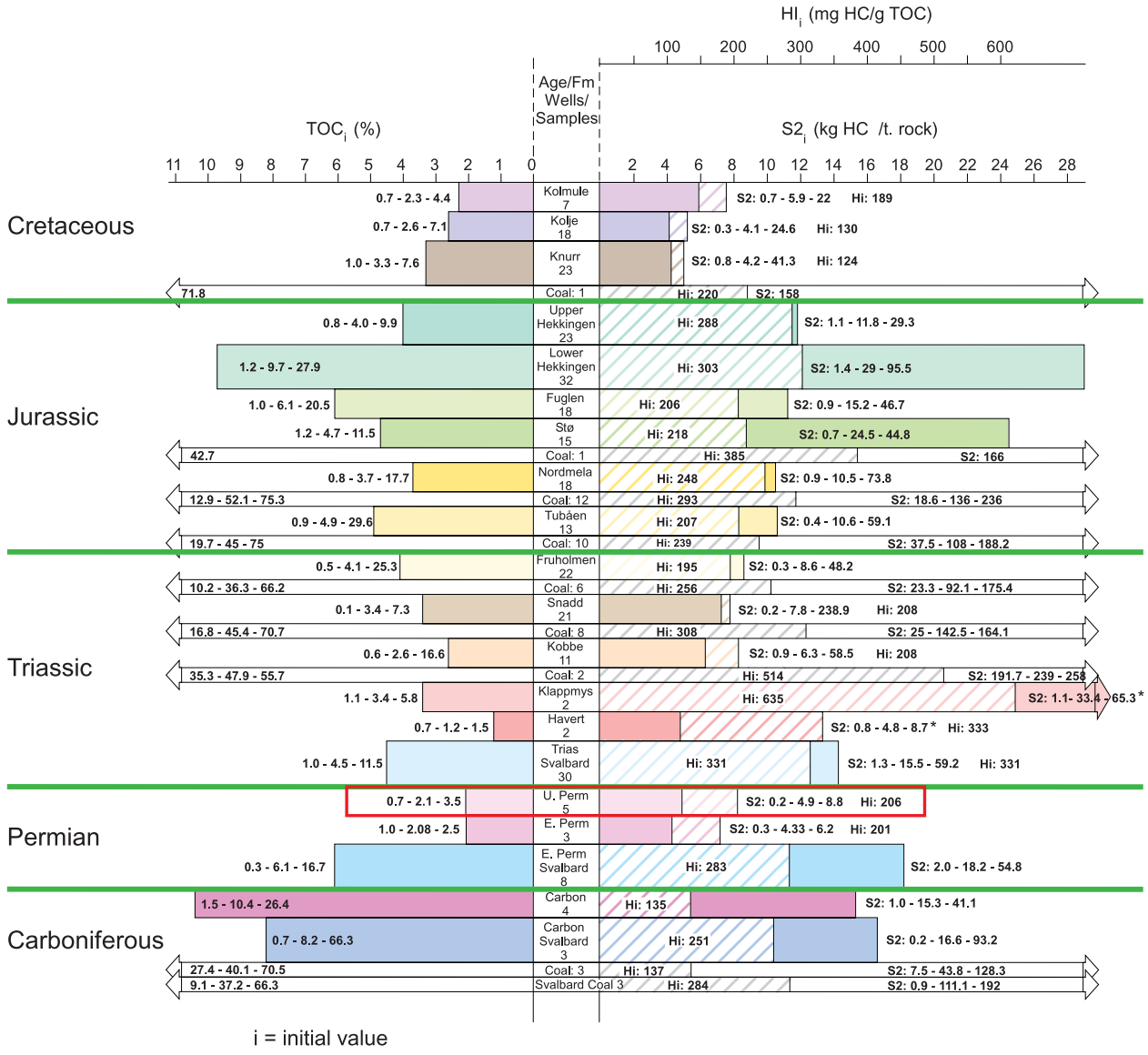

Fig. 1.6 Overview of the TOC values represented in the Barents Sea. (Ohm et al., 2008)

1.4.2 Hekkingen FM

Hekkingen FM is a black organic-rich shale from the Upper Jurassic - Lower Cretaceous, it contains a mix of Type II and III organic matter with good to excellent gas and oil generation potential. The Hekkingen FM is present on a regionally scale but its maturity differs; in the Fingerdjupet and Hammerfest basins the Hekkingen FM is oil to gas mature, this is also the case on the eastern rim of the Bjørnøyrenna Fault Complex. On the Loppa High, Bjarmeland Platform, Nordkapp Basin and on the Finnmark Platform the Hekkingen FM is immature or very early mature. In the Sørvestnaget and Bjørnøya basins the Hekkingen FM is dry-gas mature to over-mature (Thiessen, 2013).

Maximum Hekkingen FM properties ("Lower Hekkingen" on Fig. 1.6) will be used in the basin modelling as a comparison-model to the potential Palaeozoic source-rock, to get a better overview of how big the potential of the investigated Palaeozoic source rock is.

1.5 Basin modelling

"Basin modelling is forward modelling of geological processes in sedimentary basins over geological time spans" (Hantschel et al., 2009). Basin modelling incorporates deposition and compaction, pore pressure calculation, temperature determination and heat flow analysis (Fig. 1.7). In this paper parameters such as vitrinite reflectance and hydrocarbon generation will be calculated, but general basin modelling also determines adsorption and expulsion processes, fluid analysis and also migration (Hantschel et al., 2009).

There are two types of basin modelling; 1-D modelling and 2-D and 3-D fluid flow modelling (Waples, 1998), in this thesis 1-D modelling (also known as maturity modelling) will be used to determine the source potential of the Palaeozoic interval in the Loppa High area.

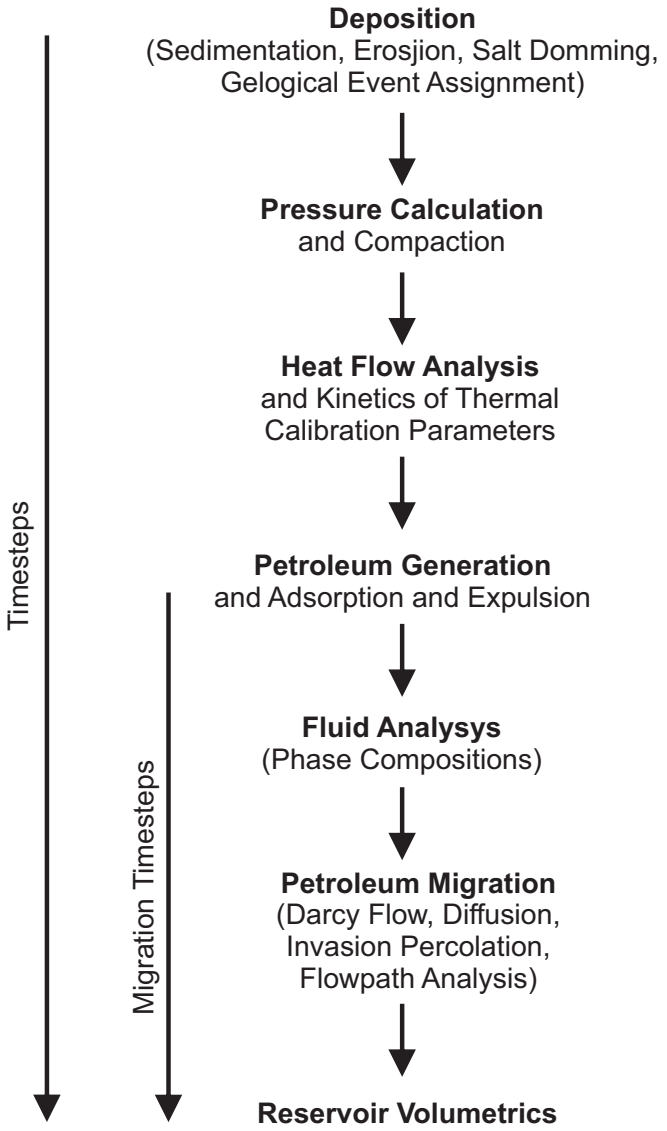

Fig. 1.7 Major geological processes in basin modeling. This study will use the investigate the three first steps in this figure. (Figure from Hantschel et al., 2009)

2 Geological background

2.1 Tectonic development

The Barents Sea can be divided into two mayor geological provinces; the western Barents Sea and the eastern Barents Sea. These two provinces are divided by a monocline structure located in the central Barents Sea. The two geological provinces in the Barents Sea have widely different geological histories; the eastern province is mainly affected by the Uralian orogeny, the Timan-Pechora Basin and the complex tectonic history of Novaya Zemlya, while the western province is mainly affected by the major post-Caledonian rifting episodes (Smelror et al., 2009).

The tectonic framework of the south-western Barents Sea is relatively complex. This region has been affected by several periods of tectonism after the Caledonian Orogeny. Due to sparse well coverage in the western basins, not much of the pre-Cretaceous history in the area is actually known.

2.1.1 Paleozoic

The eastern Barents Sea went from being a stable, passive continental margin to an active margin during late middle to early Devonian. During this time, the Uralian oceanic crust entered a progressive westward subduction ending with the Uralian orogeny culminating in late Permian. This subduction phase also led to extension in the Timian-Pechora Basin (Smelror et al., 2009).

In the western Barents Sea, the metamorphic basement developed during the Caledonian orogeny which culminated in early Devonian time (~400 Ma) (Faleide et al., 1984; Gudlaugsson et al., 1998; Smelror et al., 2009). The Caledonian orogeny was a result of the consolidation of the Baltican and Laurentian plate, and the closure of the Iapetus ocean (Fig. 2.1 A) (Gernigon et al., 2013). The best evidence for the Caledonian orogeny is found on Svalbard where we can find N-S exposed bedrock of this age (Smelror et al., 2009). In early Devonian (Lochovian), the southwestern Barents Sea was dominated by extension and large scale erosion of the the hinterlands (Smelror et al., 2009). The Late Devonian-Carboniferous rift phase (Fig. 2.1 B) was dominated by a left-lateral shear regime with large-scale strike-slip movements which formed rift zones up to 300 km wide and 600 km long in a north-easterly direction (Gudlaugsson et al., 1998; Smelror et al., 2009). From Early to Middle Carboniferous the earlier lateral shear regime shifted into extensional rifting (Fig. 2.1 C) (Faleide et al., 1984). In Late Carboniferous, the rifting ceased and the new regime indicated regional subsidence and sediment accumulation (Gudlaugsson et al., 1998).

By Late Permian a rift system between Norway and Greenland was developing and a seaway opened from northwest European basins in the south to the Arctic in the north (Fig. 2.1 D), this significant extensional event marks the Late Permian-Early Triassic transition. The consequences were increased subsidence in the western Barents Sea and amplifying of the relief of the paleo-Loppa High (Faleide et al., 1984; Glørstad-Clark et al., 2010). During late Permian there were a

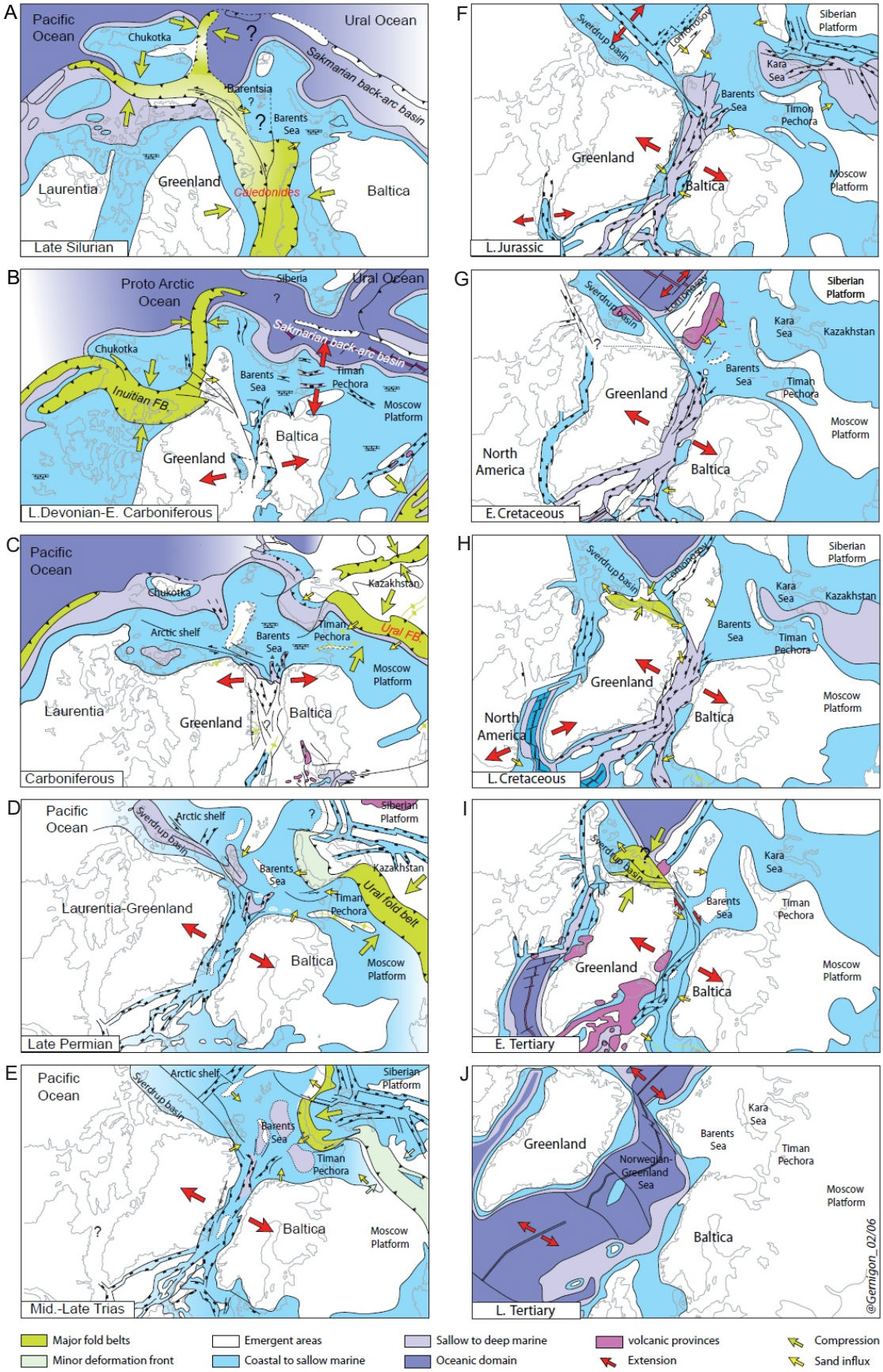

Fig. 2.1 Schematic overview of the geodynamic evolution in the Arctic region. (Ziegler, 1988).

shift in depositional environment to clastic sediments, these came in as a result of uplift of the landmasses to the south and the Uralian Mountains in the southeast (Larssen et al., 2002; Glørstad-Clark et al., 2010).

2.1.2 Mesozoic

The early Mesozoic (Triassic) was a quiet tectonic period This was followed by late Middle Jurassic-Early Cretaceous widespread rifting (Fig. 2.1 E) (Glørstad-Clark et al., 2010). The tectonic activity occurring during this rifting can be divided into two main phases; the Mid-Kimmerian tectonic phase and the Late Kimmerian tectonic phase (Faleide et al., 1984). The Mid-Kimmerian (Middle to Late Jurassic)(Fig. 2.1 F) is related to the opening of the central Atlantic Ocean, while the second phase, the Late Kimerian (Late Jurassic to Early Cretaceous) is dominated by development of large deep-rooted normal faults along zones of weakness in the Caledonian basement (e.g. the Ringvassøy-Loppa Fault Complex). During this second phase lateral variations in subsidence occurred in the southwestern Barents Sea (Faleide et al., 1984).

In the Early Cretaceous regression caused by uplift continued (Fig. 2.1 G)(Faleide et al., 1984; Smelror et al., 2009), the Northern Barents Sea was uplifted and sediments from the uplifted continental areas in the northeast were abraded into deeply subsiding basins in the west (Gernigon et al., 2013). The Loppa High was inverted in latest Jurassic-earliest Cretaceous times and remained an island throughout the Cretaceous (Clark et al., 2013). The main phase of subsidence took place towards the end of Early Cretaceous when the Late Kimmerian fault movements had (mostly) ceased (Faleide et al., 1984).

The rifting of the western Barents Sea continued in the Late Cretaceous (Fig. 2.1 H)(Clark et al., 2013).

2.1.3 Cenozoic

In the early Paleogene period the area between Norway and Greenland was progressively taken up by strike-slip movements within De Geer Zone (Fig. 2.1 I) (Smelror et al., 2009; Gernigon et al., 2013) and together with deformation it ended with the formation of pull-apart basins in the westernmost parts of the Barents Sea (Faleide et al., 1993). The Paleocene-Eocene transition is marked by the break-up of the North Atlantic margin and the opening of the Norwegian-Greenland Sea (Smelror et al., 2009). The separation of the Atlantic continued and towards the Miocene the Fram Strait was opened leading to a North Atlantic-Arctic marine connection (Fig. 2.1 J) (Faleide et al., 1984).

2.2 Depositional environments

In Early Devonian time (Lochkovian) (Fig. 2.2), the western Barents Sea was a highland, and as such, the area was undergoing denudation. Even though marine environments became more and more prominent towards the western Barents Sea (the eastern Barents Sea had a marine environment), the south western Barents Sea remained a highland throughout Devonian times (Smelror et al., 2009).

In mid Early Carboniferous times (Visean) (Fig. 2.2) a shift in the environment occurred. What had previously been a highland with some lacustrine/fluvial areas, was turning into a marsh environment. And in mid Late Carboniferous (Moscovian) (Fig. 2.2) the sea overtook the highlands. The northward drifting of Pangea also led to a change in climate during the Moscovian, the Barents Sea was no longer tropical humid but semi-arid and arid. This new influx of seawater in the western Barents Sea, combined with the climate change resulted in an expansion of the eastern carbonate shelf and widespread evaporite depositions (Smelror et al., 2009), these depositions are recognized on the lithostratigraphic chart over the Barents Sea as Ørn FM (Fig. 2.3).

The carbonate depositional environment continued throughout early Permian. In early Late Permian (Wordian) (Fig. 2.2) the climate changed from warm and arid to temperate, and the depositions changed from carbonates to siliciclastic. These siliciclastic depositions are found in Røye FM (Fig. 2.3) and are the depositions that represents the potential source rock in this thesis. The Wordian age was a time with overall transgression, leading to larger areas of deep marine environment (Smelror et al., 2009).

The depositional environment in the western Barents Sea during earliest Triassic (Induan) (Fig. 2.2) was characterised by siliciclastic sediments, assumed to be primarily from the Uralian Mountains (Glørstad-Clark et al., 2010). The south-western Barents Sea was a shallow sea at this time, and areas like Loppa High was exposed and subjects to erosion (Smelror et al., 2009).

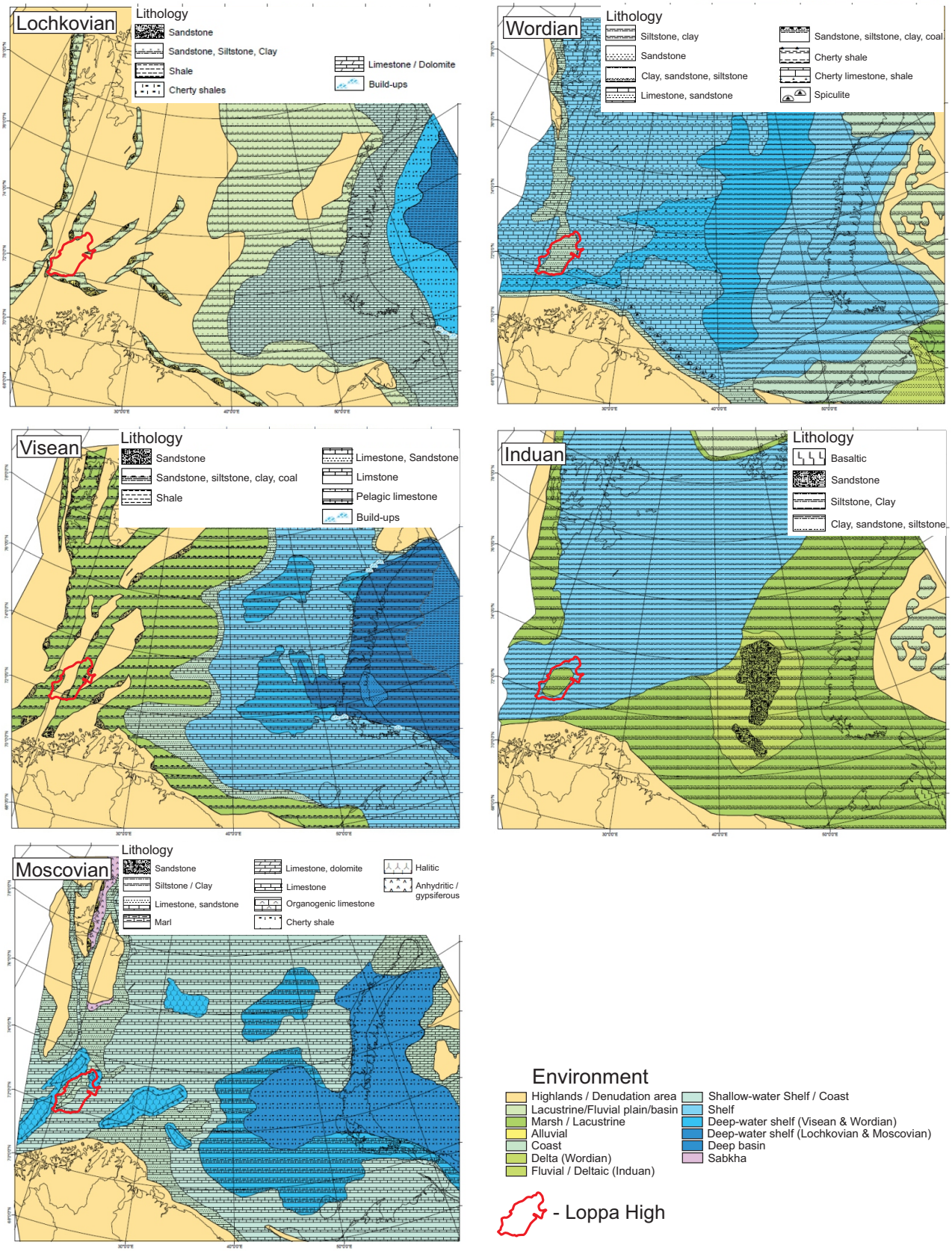

Fig. 2.2 Depositional environment in the Barents Sea from Lochkovian to Induan times. (Figure modified from Smelror et al., 2009).

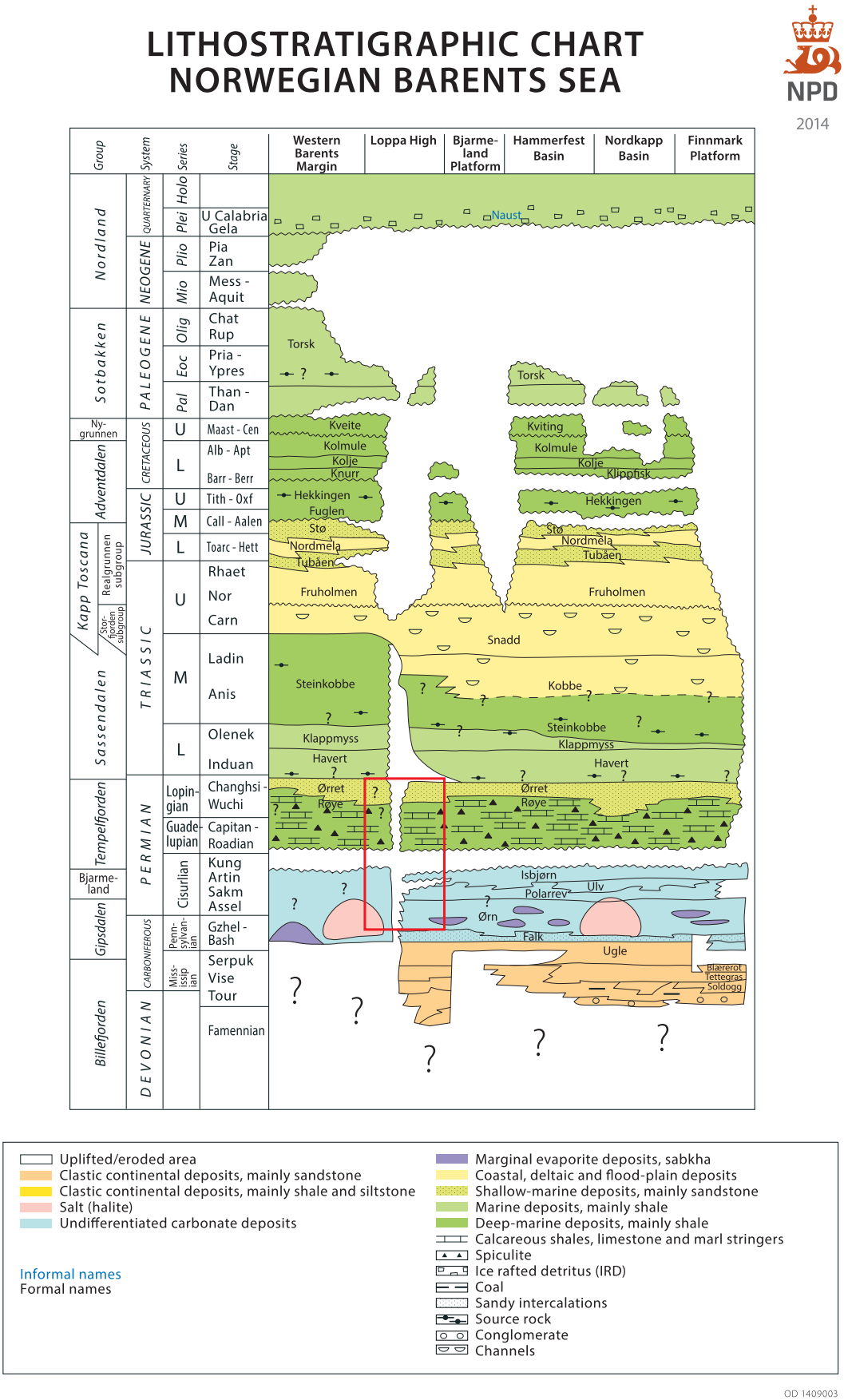

Fig. 2.3 Litostratigraphy chart over the Norwegian Barents Sea. The Palaeozoic interval that will be investigated is highlighted in the red box. (Figure made by NPD)

2.3 Stratigraphy

The stratigraphy in the Barents Sea is generally the same throughout the whole area if we focus on sediments of Triassic and older age, but Loppa High is slightly altered due to being exposed and eroded several times in its development. These "erosion scars" can be easily recognized on the Lithostratigraphic chart made by NPD (Fig. 2.3), the blank areas on this figure represent eroded strata.

BASEMENT

The basement in the south western Barents Sea is believed to consist of crystalline rocks formed during the Caledonian orogeny (Gudlaugsson et al., 1998). In the Barents Sea only 9 wells have penetrated the basement (including appraisal wells like 7220/11-2 and 7220/11-2 A), and 5 of these 9 wells are within Loppa High. Well 7120/1-1 R2 and 7120/2-1 took one core sample each in the basement, and well 7120/2-1 reports showings of an altered dolerite sequence (Basset, 2003).

GIPSDALEN GP

This group consists of the three formations Falk, Ugle and Ørn. Well 7121/1-1 R penetrated a 1000 m thick succession of Gipsdalen GP sediments on the southern flank of Loppa High. The group is generally showing shallowing upward trends, continental red bed sandstones, siltstones and conglomerates in the lower part of the succession. Further up mixed carbonates and grey-coloured marine sandstones are found before the whole sequence is topped off with rhythmically bedded limestones and dolomites with minor evaporites on the platform areas (Larssen et al., 2002).

BJARMELAND GP

The Bjarmeland GP also consists of three formations; Isbjørn, Polarrev and Ulv. The thickest succession of this group can be found at the eastern flank of Loppa High were it is 488 m thick in well 7121/1-1 R. The lithology in the Bjarmeland GP is dominated by white to light grey bio-clastic limestones and some local bituminous limestones. In the uppermost parts there are also small amounts of cherts (Larssen et al., 2002).

TEMPELFJORDEN GP

Only two formations occur in this group, these are Røye FM and Ørret FM. Its thickest succession can be found along the southern margin of the Hammerfest Basin where it is 901 m in well 7120/12-2. The thickest succession on Loppa High is found in well 7120/1-1 R2 were it is 591 m thick. The lithology is characterised by dark to light grey spiculites, spiculitic cherts, silicified skeletal limestones and fine-grained siliciclastic (Larssen et al., 2002).

2.4 Structural elements

The Loppa High has a diamond shaped outline and is a marked N-S trending structural feature (Gabrielsen et al., 1990). It is surrounded by sedimentary basins and stands out from surrounding basins as a marked isolated structural high. It is located near the southwestern margin of the Norwegian Barents Sea (Fig. 1.2) (Sayago et al., 2012).

Loppa High is separated from the Tromsø and Bjørnøya basins to the west by the Bjørnøyrenna and Ringvassøy-Loppa Fault Complexes, from the Hammerfest Basin in the south by the E-W trending Asterias Fault Complex and to the east it grades into the Bjarmeland platform (Halland et al., 2013).

The Loppa High also incorporates two other structural elements (Fig. 2.4), the Svalis Dome to the north and the Polheim Sub-platform to the west (Gabrielsen et al., 1990).

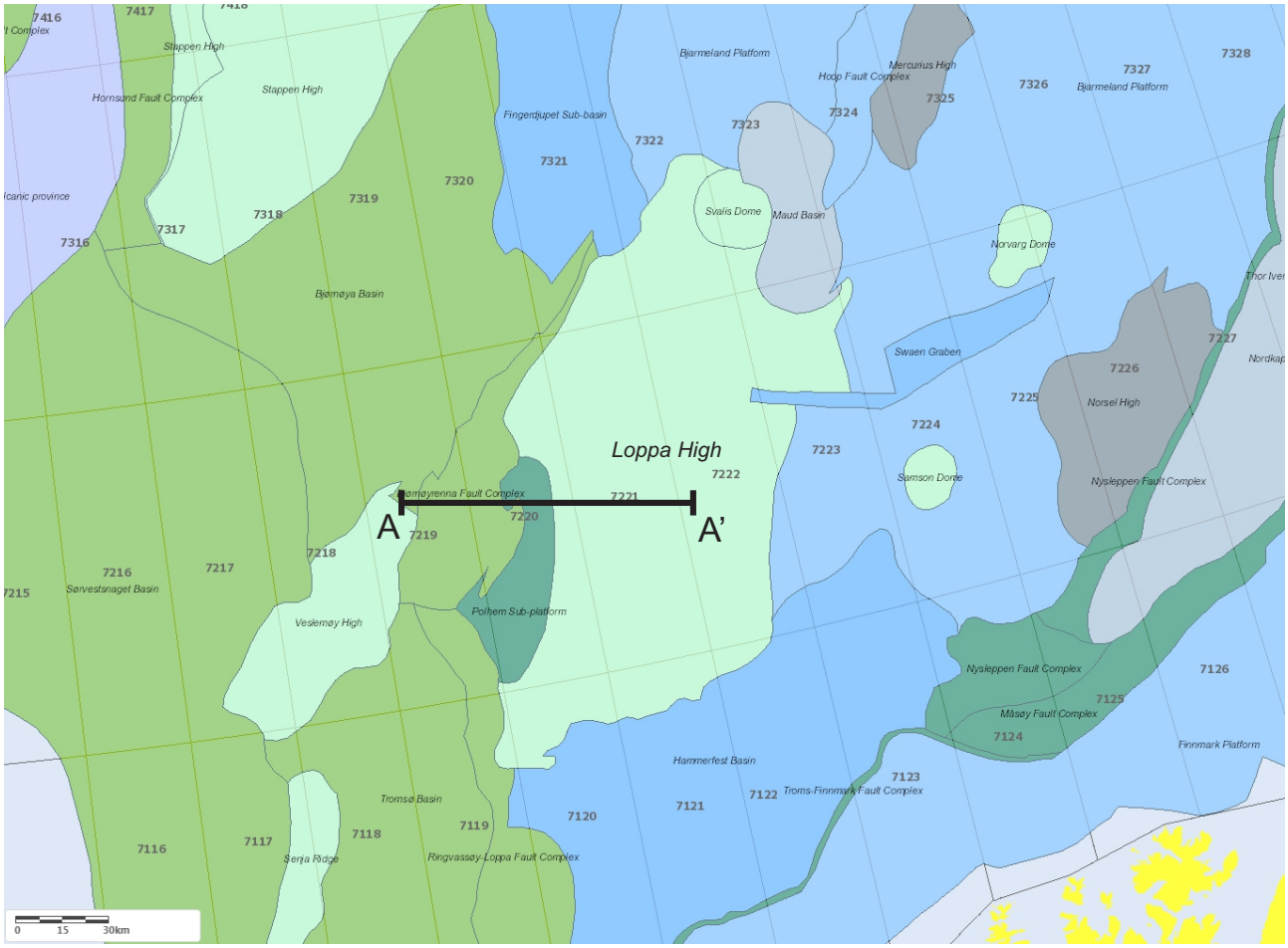

Fig. 2.4 Structural elements in the western Barents Sea. A-A' cross section can be seen on Fig. 2.5.

The Loppa High is structurally complex due to several phases of uplift and subsidence followed by tilting and erosion (Fig. 2.5) (Wood et al., 1989; Halland et al., 2013). The main periods of tectonism occurred in late Jurassic to early Cretaceous and late Cretaceous to Cenozoic (Henriksen et al., 2011). Terrigenous clastics from Early Carboniferous are onlapped by Upper

Carboniferous and Permian Carbonates, which were eroded during Early Triassic (as a result of the uplift.) (Wood et al., 1989). It was then buried by a clastic sequences of Lower to Middle Triassic age (Fig. 2.5d). The Triassic and Jurassic sediments deposited on Loppa High were eroded due to a footwall uplift occurring in Late Jurassic to Early Cretaceous, this uplift made Loppa High an exposed island (Fig. 2.5c) (Wood et al., 1989).

Loppa High remained an island until early Paleocene, but after a long period of subsidence it was a again fully submerged under water (Fig. 2.5b). Closing in on the present day Loppa High, the area was uplifted and eroded again, this time it formed an unconformity with low-angle Cenozoic (and older) sediments below Quaternary glacio-marine sediments (Fig. 2.5a) (Wood et al., 1989).

Loppa High is also associated with positive magnetic and gravity anomalies caused by a relatively shallow metamorphic basement underlying its western part (Gabrielsen et al., 1990).

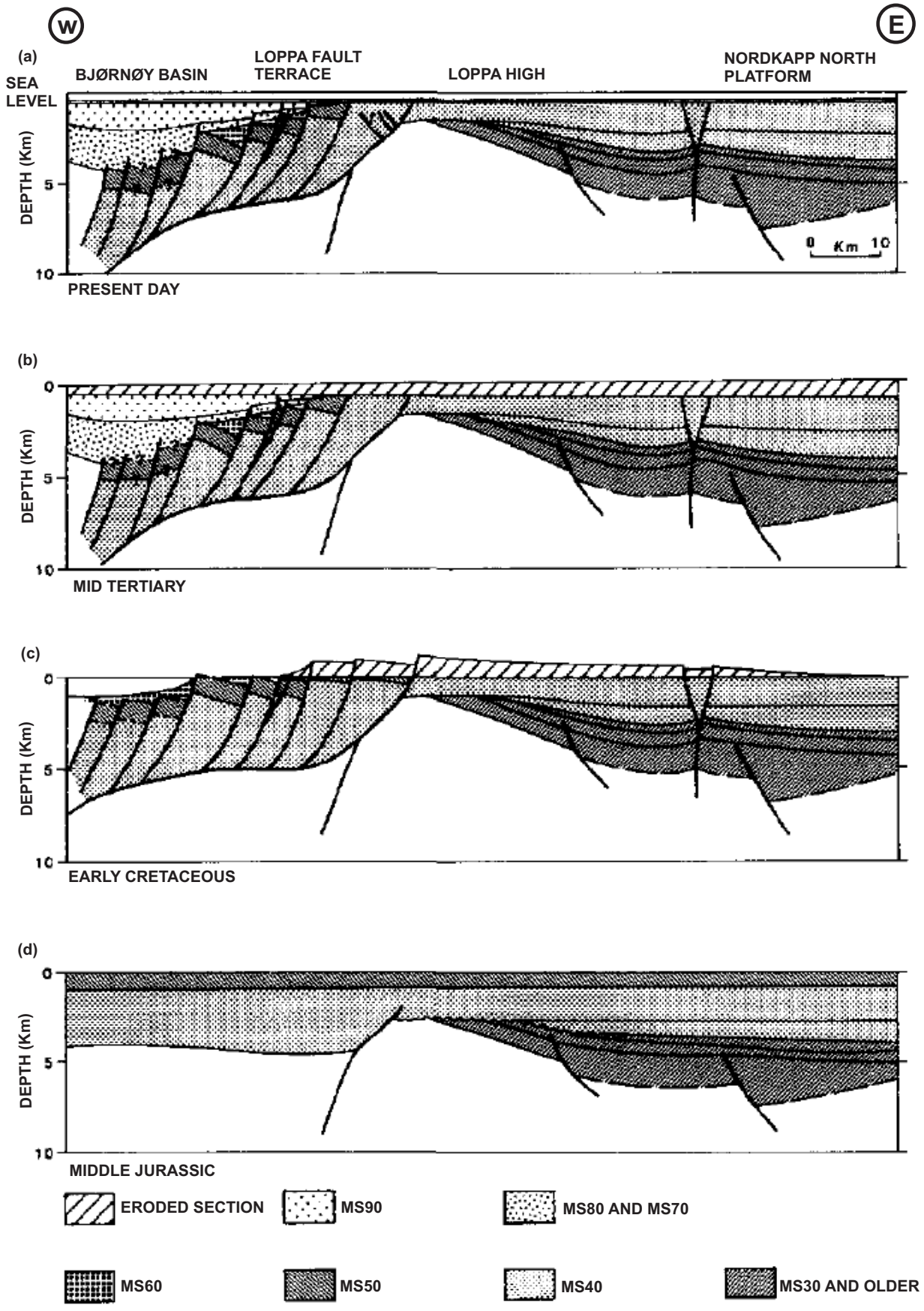

Fig. 2.5 Schematic evolution of a west-east cross section over Loppa High, line A-A' (see Fig 2.4 for approximate location). (a) Present-day structure, (b) Mid-Tertiary before late Tertiary erosion, (c) Early Cretaceous structure, (d) Late Middle Jurassic structure prerift. (Figure from Wood et al., 1989).

2.5 Glacial erosion and uplift of the SW Barents Sea

From a petroleum point of view the erosion and uplift history of an area is key, it is used to determine the quality of your reservoir and source rock (and will also effect several other factors such as the seal and leakage). The amount of sediments eroded in an area tells us something about how deep the underlying rocks have been buried. For a source rock it is key to decide how the temperature has affected the maturation and production of hydrocarbons. The maturation of a source rock is an irreversible process, so a source rocks measured maturity parameter always reflects the maximum temperature the source rock has seen (Henriksen et al., 2011).

Based on available geophysical and geological data, a study of net erosion and uplift has been carried out for the Barents Sea and the result is a regional net erosion map (Fig. 2.6). The Loppa High area has experienced a net erosion of 1400-1800 m, with an erosion uncertainty of ±150m (Henriksen et al., 2011).

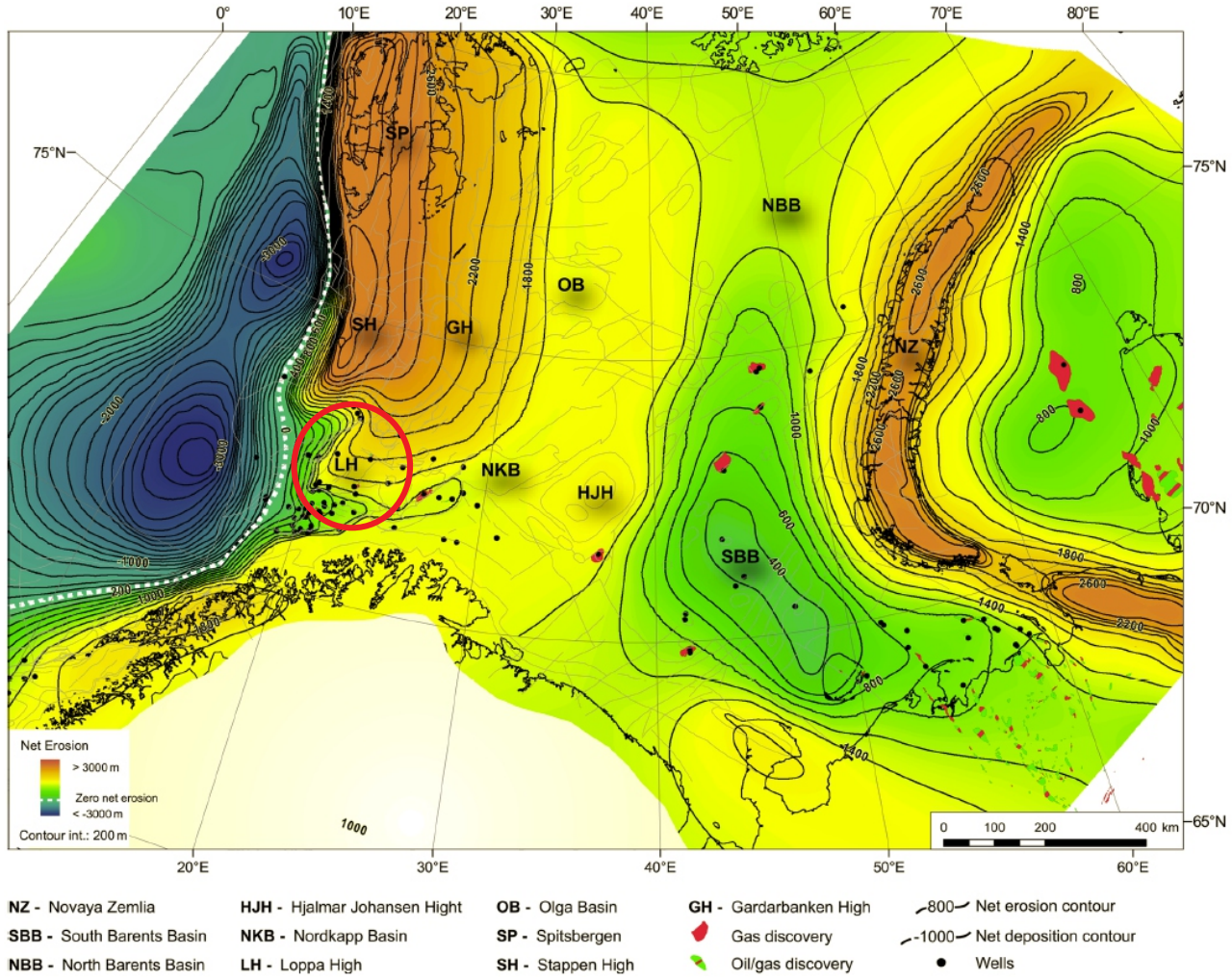

Fig. 2.6 A regional map showing the estimated net erosion for the Barents Sea. To the west of Loppa High (Highlighted in the red circle) there has been only subsidence, while the rest of the Barents Sea region has experienced erosion ranges from 0 to >3000 m. (Figure from Henriksen et al. 2011).

3 Data & Method

3.1 Data

3.1.1 Seismic data

The seismic used in this study is public seismic data gathered on the Norwegian continental shelf, it is shown on Fig. 3.1 and listed in Table 3.1.

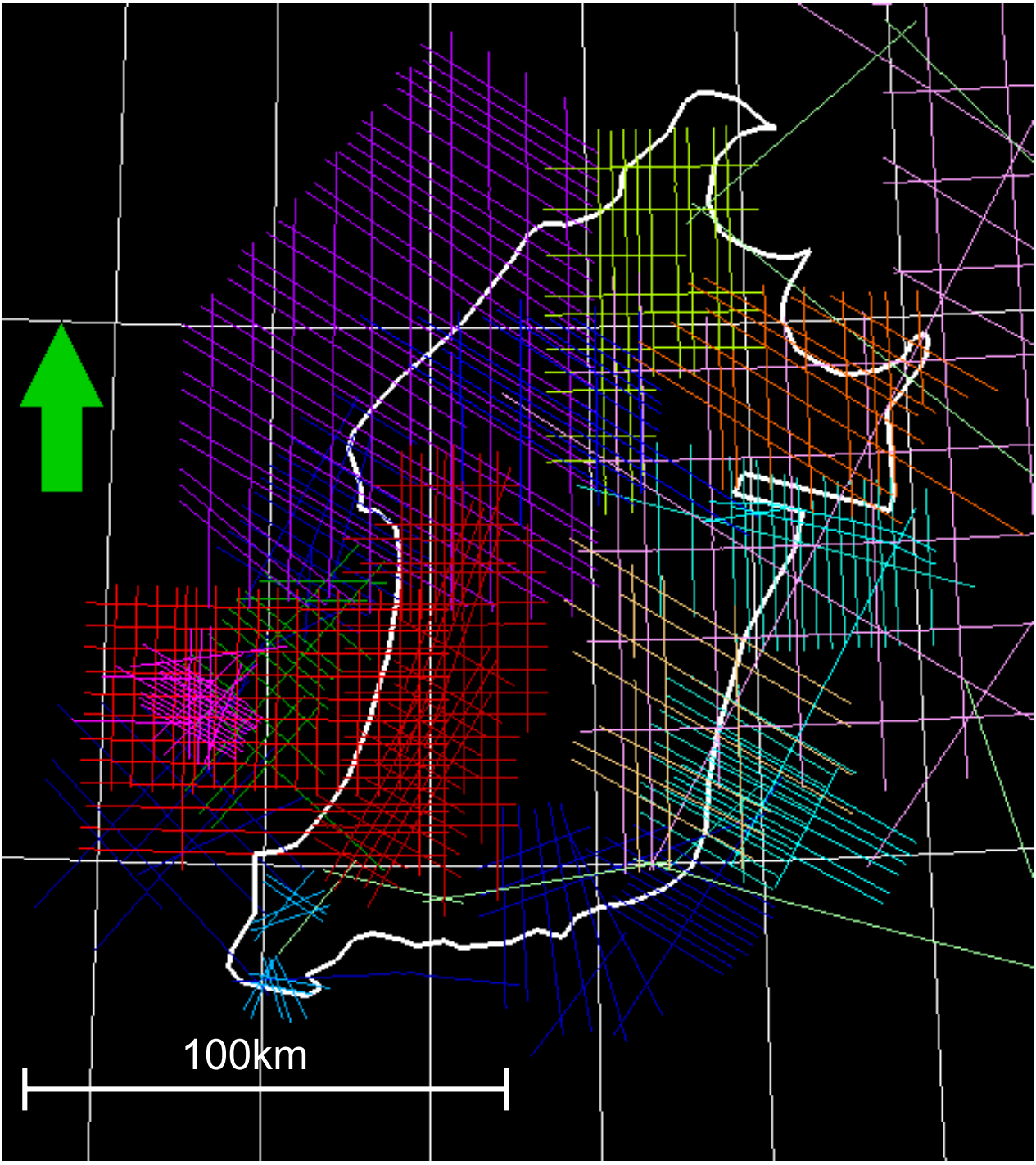

Fig. 3.1 Seismic basemap. Showing the location and coverage of seismic data used in this study.

Table 3.1 Seismic database. A list of the seismic data used in the study.

Survey name	2D/3D	Nr. of lines	Quality	Colour on map
AN-88-9Q6-4-Nordkapp Basin	2D	31	Fair	
F-86-Bjørnøya South	2D	23	Fair	
LHSG-89-Loppa South	2D	47	Good	
NH-8403-Bjørnøya South	2D	35	Fair	
NH-8506-Loppa Ridge	2D	55	Fair to good	
NH-8514-Lopparidge	2D	26	Good	
NPD-NOLO-85	2D	96	Fair	
SG-8737-Barents Sea	2D	13	Good	
SG-9309-Loppa High West	2D	50	Good	
SG-9401-Bjørnøya sør	2D	21	Fair	
SG-9714-Loppa	2D	14	Poor to fair	
SG-9715-Barents Sea	2D	11	Poor to fair	
SH-9103-Block 7120/1	2D	12	Fair	
ST-8813-Loppa High	2D	11	Fair to good	
ST-8823-Loppa High	2D	16	Fair to good	

3.1.2 Well data

The wells used in this study is shown on Fig. 3.2 and listed in Table 3.2.

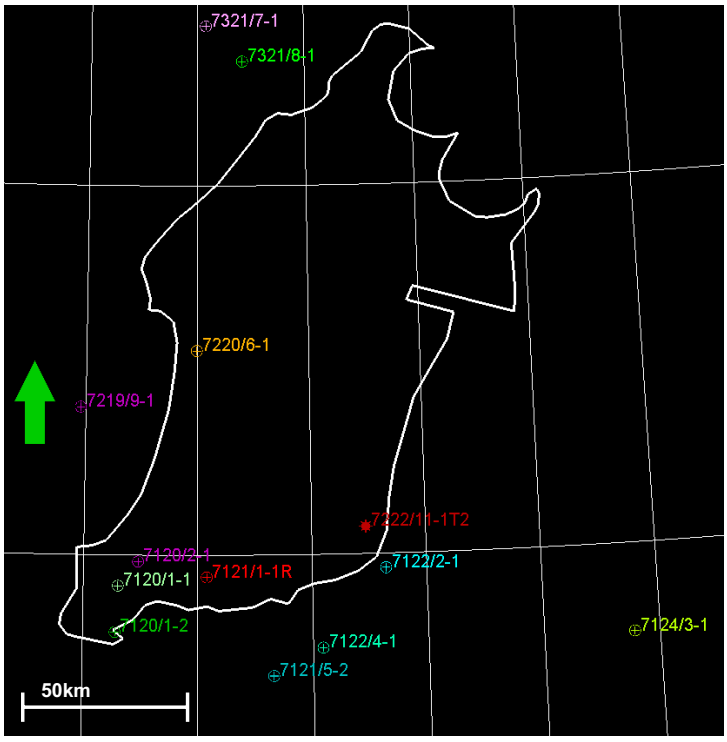

Fig. 3.2 Well basemap. Displaying the wells used in this survey.

Table 3.2 Well database. List of the wells used in this study.

Wells	Completion year	Keywells	Cretaceous			Jurassic					Triassic				Permian		Carboniferous		Oldest penetrated formation (Bold line in table)	MD (m)
			Adventdalen			Kapp Toscana							Sassendalen		Tempelfjorden		Gipsdalen			
						Realgrunnen					Stor-fjorden									
			Kolje	Knurr	Hekkingen	Stø	Nordmela	Tubåen	Fruholmen		Snadd		Kobbe	Havert	Ørret	Røye	Ørn	Falk		
7120/1-1	1985	x																	RØYE FM	2569
7120/1-2	1989																		FRUHOLMEN FM	2630
7120/2-1	1985	x																	BASEMENT	3502
7121/1-1 R	1986	x																	ØRN FM	5000
7121/5-2	1986																		FRUHOLMEN FM	2543
7122/2-1	1992																		STØ FM	2120
7122/4-1	1992																		SNADD FM	3015
7124/3-1	1987																		ØRN FM	4730
7219/9-1	1988																		SNADD FM	4300
7220/6-1	2005	x																	BASEMENT	1540
7222/11-1 T2	2008																		KOBBE FM	2658
7321/7-1	1988																		SNADD FM	3550
7321/8-1	1987	x																	RØYE FM	3482

Legend:	GasCond	Oil/Gas	Oil	Oil Shows	Gas	Gas Shows	O/G Shows

3.2 Seismic resolution

Seismic resolution tells us something about the amount of stratigraphic detail it is possible to extract from seismic data. There are two aspects of seismic data resolution - vertical and horizontal resolution. Both of these depend on the wavelength, velocity and frequency of the signal. The resolution depends on the seismic wavelength which is determined by the formula $\lambda = v/f$ (λ = wavelength (m), v = acoustic velocity (m/s), f = frequency (Hz)) (Sheriff, 1985).

With increasing depth all the parameters in the formula is affected resulting in lower resolution (Fig. 3.3). The wavelength increases, the velocity increases (due to higher degree of compaction and burification) and the frequency decreases due to higher frequencies attenuates at a high rate than lower frequencies (Sheriff, 1985; Brown, 1999).

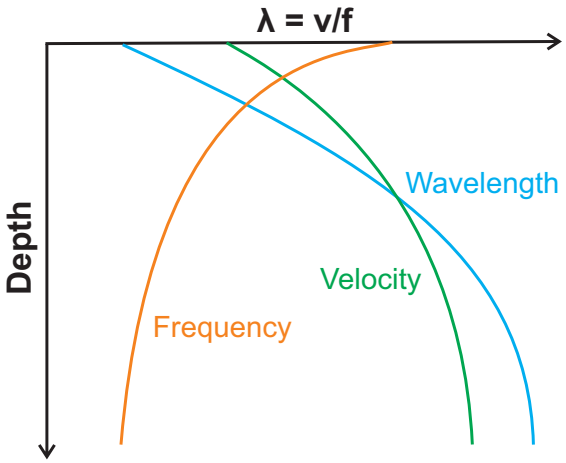

Fig. 3.3 The change of frequency, velocity and wavelength pf the seismic signal with increasing depth. (Brown A. R., 1999.)

3.2.1 Vertical resolution

The vertical resolution is defined as the minimum thickness a layer must have in order to be distinguished as a separate layer in a seismic section, and the equation is given as Vr = λ/4 (Vr = vertical resolution, λ = wavelength). If the layer thickness is more than half of a wavelength, the reflections will not interfere and two separate reflections will be produced. For a thickness approaching a quarter wavelength, the reflection will interfere constructively creating a single reflection with increased amplitude. If the thickness decrease even further, down to lower than a quarter of a wavelength, the reflections will interfere destructively leading to the two reflectors reducing each others amplitude, and this reduction will increase until it reaches the limit of visibility at λ/30 (layers thinner than that will not be visible) (Sheriff, 1999).

Vertical (and horizontal) resolution for a limited selection of surveys can be seen in Table 3.3, the peak frequency is picked in areas on the seismic line where interpretation have been carried out, and where there also have been a well present to help pick thee velocity.

Table 3.3 Vertical and horizontal resolution for a few key seismic lines used in the interpretation.

Dataset	Seismic line	TWT (ms)	Velocity (m/s)	Frequency (Hz)	Wavelength (m)	Vertical resolution (m)	Horizontal resolution (m)
SG9309	305	2320	3880	35	82.3	20.6	499.5
NH8506	405	1080	5147	28	183.8	28	505.4
SG8737	101	1884	4753	23	206.7	51.7	680.3

3.2.2 Horizontal resolution

Horizontal resolution is the horizontal distance needed in order to separate two elements from each other. The extent of the zone reducing the reflection is widely know as the Freznel zone (Fig. 3.4a). The first Fresnel zone is defined as the area of the reflector from which energy returns to the

detector within a half-cycle of the reflection (Fig. 3.4b). The radius of the Fresnel zone is rf = (v/2)*(√(t/f)) (rf = radius of the Fresnel zone, v = average velocity, t = two way travel time, f= dominant frequency.) (Sheriff 1985)

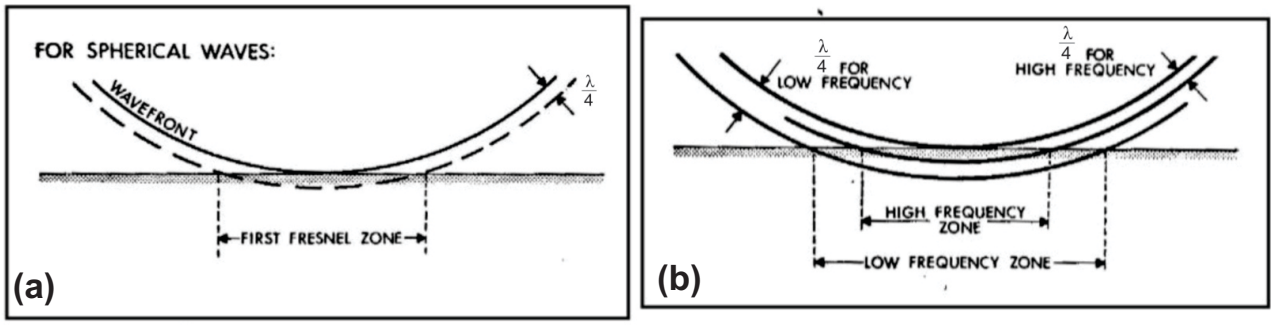

Fig. 3.4 Fresnel zone. (a) The first energy to reach the receiver from a horizontal reflector is from the point where the reflector is first tangent to the wavefront. The area of the reflector that produces the reflection is restricted by the area that the wavefront λ/4 wavelength later makes with the reflector. (b) The Fresnel zone will be larger for low-frequency components than for high-frequency components. Figure modified from Sheriff R. A., 1985.

One way to improve the horizontal resolution is through migration, which reduces the Fresnel zone (Fig. 3.5). 2D-migration will reduce the Fresnel zone to an ellipse perpendicular to the 2D-line, and 3D migration reduces the zone to a small circle around the seismic line (Brown, 1999).

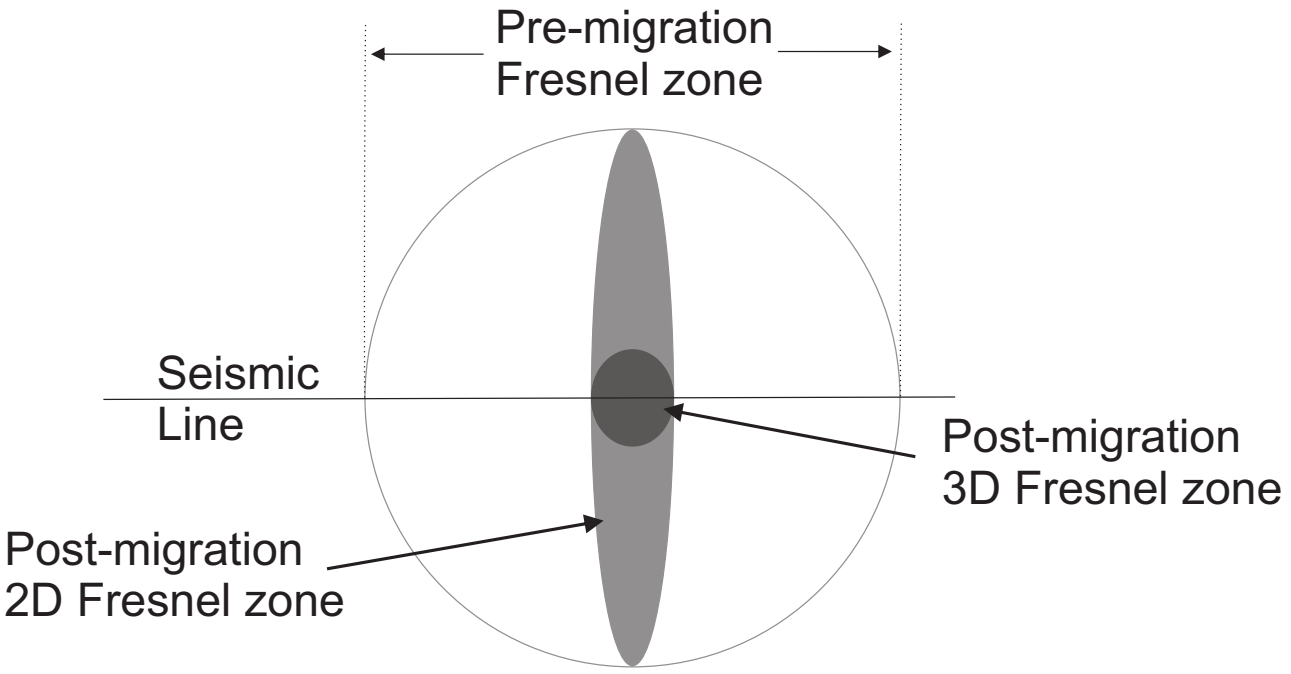

Fig. 3.5 An illustration of the Fresnel zone before and after migration. Figure modified from Brown, A. R., 1999.

Horizontal resolution for a selection of surveys can be seen in Table 3.3.

3.3 Method

3.3.1 Petrel

Petrel E&P Software Platform is a tool used by E&P companies all over the world. It is made by Schlumberger, a oilservice-company regarded as a leading force in technical solutions within exploration and production. Petrel was developed in 1996 and through several versions with step by step improvements to its algorithm it has become the product it is today. In this theses the 2016-version of Petrel has been used.

3.3.2 Petroleum Systems Quick Look

"Petroleum Systems Quick Look" (from now on referred to as PSQL) is a simple basin modelling tool in Petrel. PSQL evaluates the charge potential of a potential source rock by performing a quick look assessment of the age, geochemistry and thermal conditions in a basin. It models the maturity of a potential source rock and how it changes with different values in geochemical and thermal input. The module has 4 different "stages" (Fig. 3.6) and this thesis focuses on "Make generation properties", which is the stage that defines the properties of the source rock. The other stages goes further into the complete petroleum system, and focuses on reservoir, seal and the charge potential/flow path.

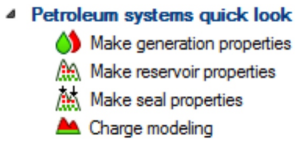

Fig. 3.6 Tools within the PSQL-module

Input

There are three input panes; "Depth/Age" (Fig. 3.7), "Geochemistry" (Fig. 3.8) and "Thermal" (Fig. 3.9). The depth/age tab uses interpreted surfaces to define the source rock, while the geochemistry and thermal tab requires theoretical input such as TOC and thermal gradient, this information needs to be taken from an external source.

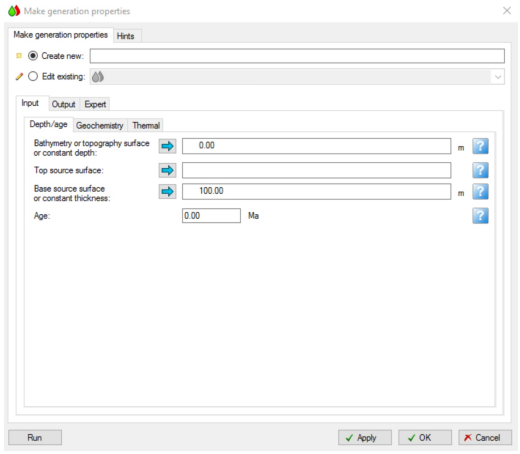

Fig. 3.7 PSQL Input pane "Depth/Age".

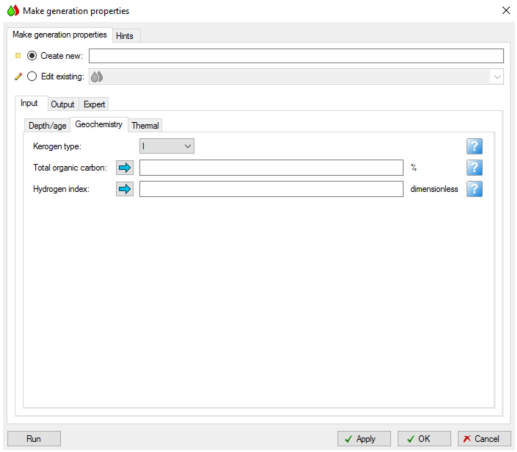

Fig. 3.8 PSQL input pane "Geochemistry".

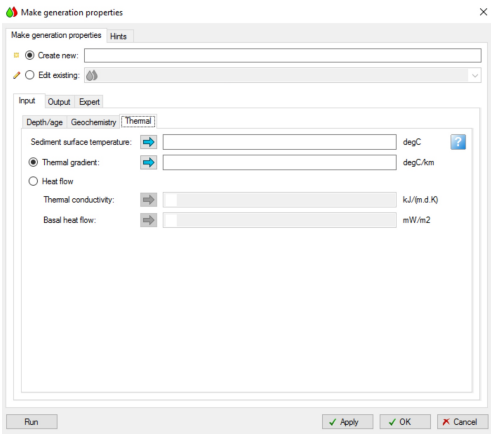

Fig. 3.9 PSQL input pane "Thermal".

Output

There are two output panes; "General" (Fig. 3.10) and "Timing" (Fig. 3.11). The "General" tab is optional and have not been used. The "Timing" tab is where you change the percent value of e.g. vitrinite reflectance, for instance if the entrance in main oil window value is set at 1% of vitrinite reflectance it will show a specific colour on the surface in all areas that has values above 1% (and up to the entrance of the "Late oil window"). The values set as standard in Petrel follows the general consensus in the industry and have therefore not been changed.

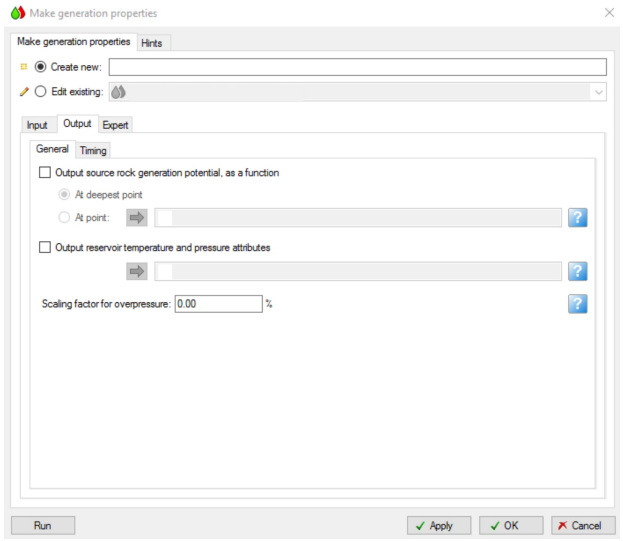

Fig. 3.10 PSQL Output pane "General"

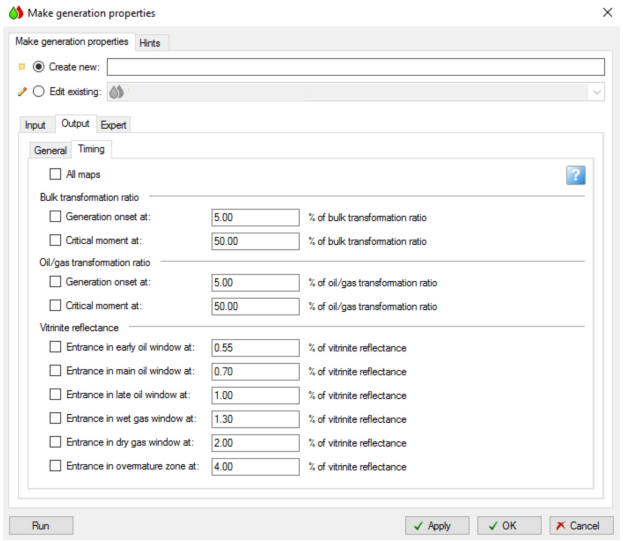

Fig. 3.11 PSQL Output pane "Timing"

Expert

The last pane is called "Expert" (Fig. 3.12). The key part to notice in this pane is the "Burial history" part, which is critical when examining a potential source rock. For this thesis there were no Petrel available burial history, so the applied burial history will be elaborated in the result chapter as a erosion-correction.

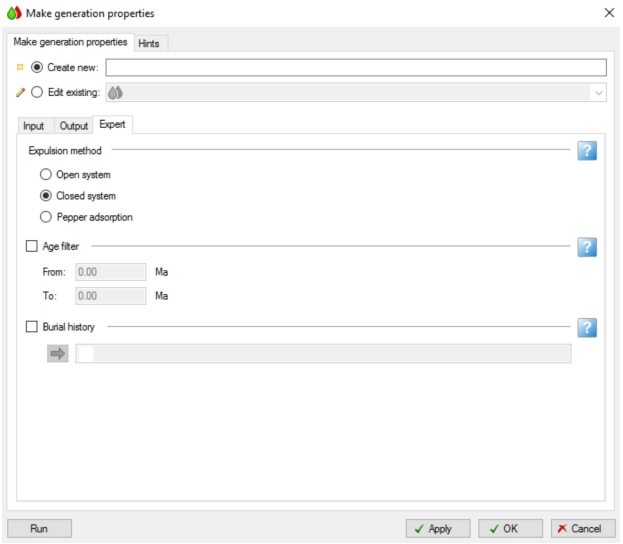

Fig. 3.12 PSQL "Expert" pane.

3.3.3 PSQL input values

A total of 30 different models have been carried out for the interpreted source rock, from these the following selection will be displayed in the result chapter; P10, P50, P90, and a comparison model where the input values used are from Hekkingen FM is also included (Table 3.4). The P50-model values have been used in two extra models, one that used the source rock at a depth 150m deeper than the rest of the models, and one that used the source rock at a depth 150m shallower than the rest of the models, this was done to see how the model would respond to changes in source rock depth (the 150m value is taken from the erosion-uncertainties on the depth-correction that was carried out - see Chapter 4.1.3). Sediment surface temperature is set to 4°C for all models.

Table 3.4 Input values for the PSQL module.

	P10	P50	P90	Hekkingen
TOC[1] (%)	0.7	2.1	3.5	27.9
HI[2]	200	275	330	300
Thermal gradient (°C/Km)[3]	25	30	35	30
Age (Ma)[4]	272	272	272	272
Kerogen (%)[5]	Type II	Type II	Type II	Type II

[1]Ohm et al. 2008.

[2]Henriksen et al. 2011a.

[2]Khutorskoi et al. 2008.

[4]Based on cores from well 7128/12-U-01 and 7129/10-U-01.

[5]Based on the depositional environment around Loppa High during Permian times.

4 Results

The result chapter will first go through the interpretation of the source rock, which includes looking at a couple of key seismic lines used to define Top Ørn and Top Røye in the Loppa High area. It will also include a more detailed explanation of the net-erosion correction that was carried out on the source rock, before moving over to the result of the PSQL modelling. There have been carried out a total of 28 models, and 4 of these will be looked into in more detail. These six models includes a minimum value model (P10), a medium value model (P50), a maximum value model (P90), and a model that uses input values from the Hekkingen FM**.** Lastly the generation potential from 26 models will be shown.

4.1 Interpretation of the source-rock

4.1.1 Top Ørn FM

The potential source rock in the Palaeozoic interval in the Loppa High area is assumed to be the Permian interval where top Ørn FM defines its bottom (<broken cross-reference>).

The interpretations are based on well tops from well 7120/2-1 (NPD, 1985), 7121/1-1 R (NPD, 1986), 7124/3-1 (NPD, 1987) and 7220/6-1 (NPD, 2005). The top Ørn reflector is a peak but the amplitude is low, and it rarely stood out compared to surrounding reflectors.

Well 7120/2-1 and 7121/1-1 R are the two key wells for the interpretation of Top Ørn FM, these wells are located in the southwestern part of Loppa High. Line 102 from the seismic survey "SG-8737-Barents Sea" (Fig. 4.1) shows both of these wells, and is a good example of the west-east dip the surface has. Another important feature on this line is the termination of the Top Ørn surface, because this truncation is the furthest west Top Ørn is present in the available dataset.

As mentioned, well 7121/1-1 R was one of two starting points, this well also shows Top Ørn on Line 305 in the seismic survey "SG9309" (Fig. 4.2), this seismic line shows the South-North trend in the eastern parts of the interpreted source rock. The surface is dipping downwards from north towards south with a peak height around trace 2139, which is the shallowest point of the surface.

Looking at Top Ørn further north and in the west-east direction (Fig. 4.3) one might see that the horizon dips from west towards east. The high in the west is affected by faults while the eastern parts have a steady dipping trend until the edge of the Loppa High area around trace 8854 where it dips steeper. From north to south in the central-eastern parts of the interpreted Top Ørn horizon, a steady dip with a low gradient from north to south is present (Fig. 4.4), the horizon is smooth except for the northern part which is affected by two faults.

Line 408 from the seismic survey "ST8813" (Fig. 4.5) shows the northwest-southeast trend in the central-eastern area, this area has a steady dip with a slightly higher gradient than the N-S dip, and is clearly showing the edge of Loppa High as a big dip around trace 1309.

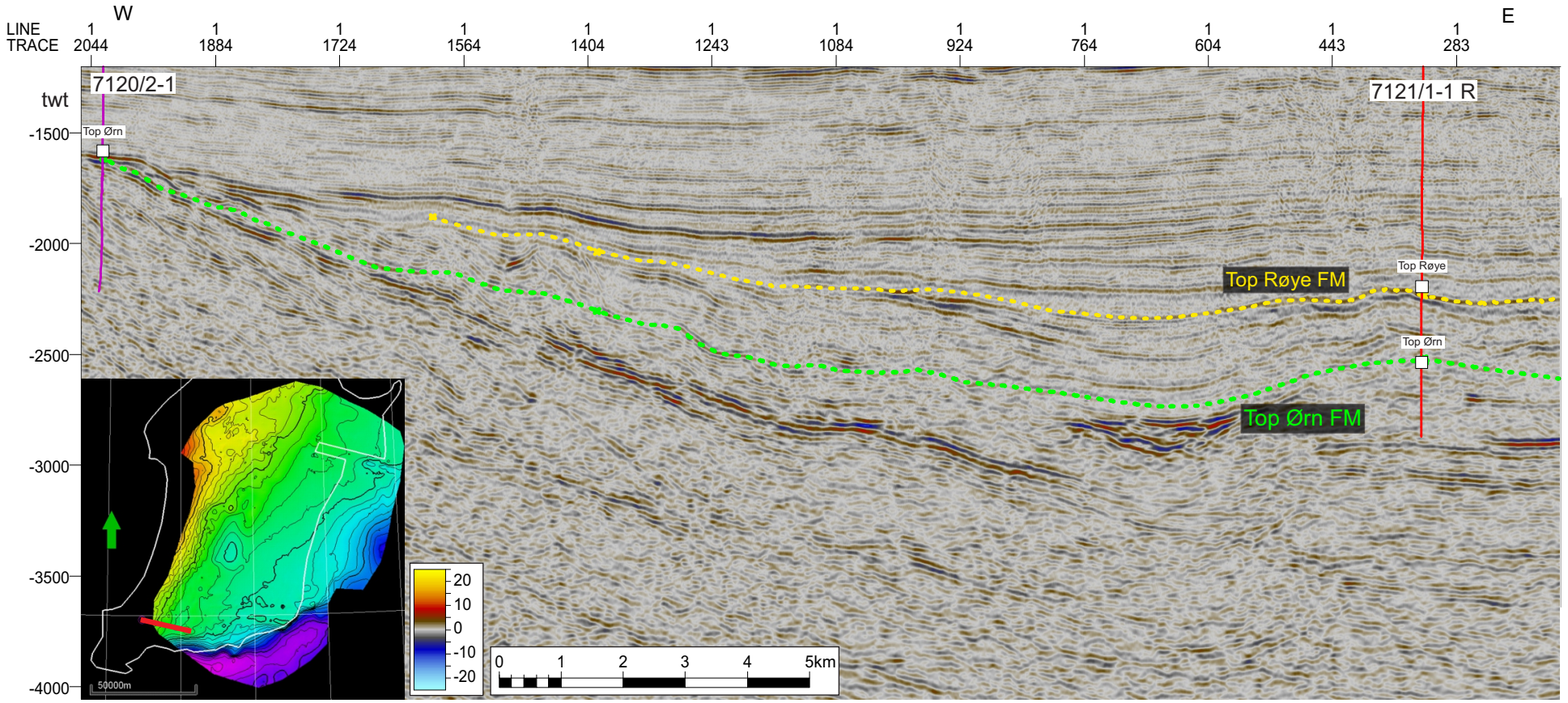

Fig. 4.1 Intepretation of Top Ørn and Top Røye on line 102 from seismic survey "SG-8737-Barents Sea" based on well tops from well 7120/2-1 and 7121/1-1 R. The placement of the seismic line is highlighted as a red line on the Top Ørn surface in the bottom left corner (same for all seismic profiles).

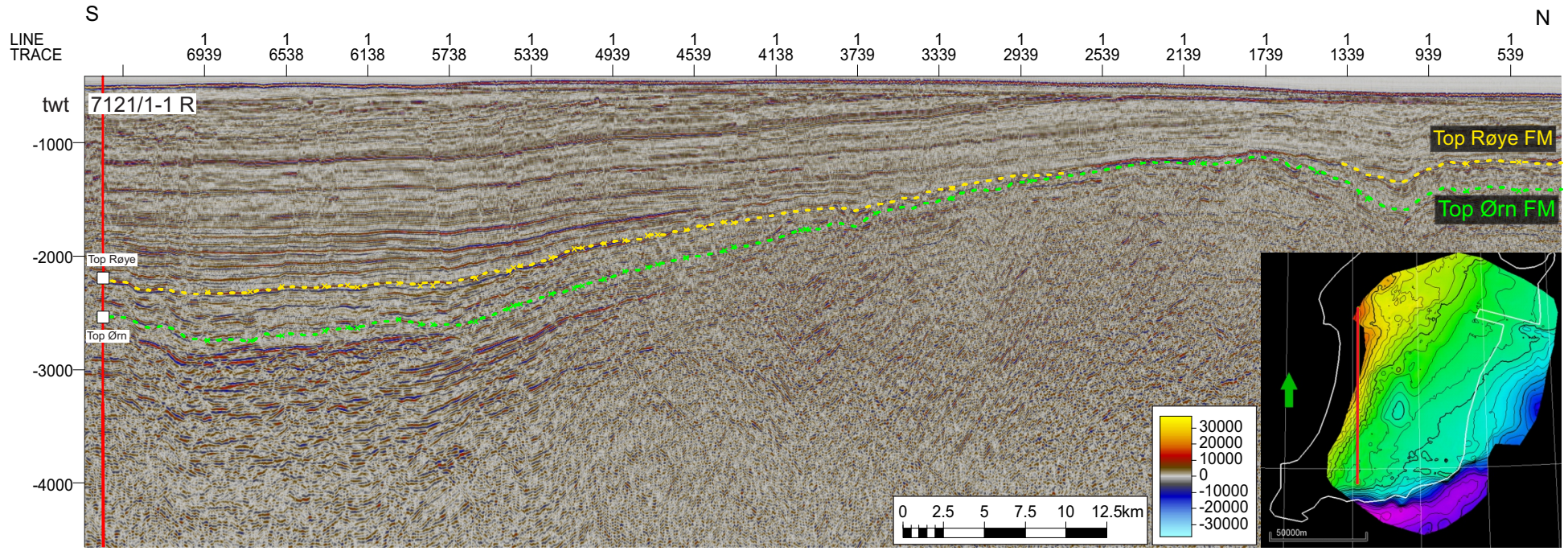

Fig. 4.2 interpretation of Top Ørn and Top Røye on line 305 from seismic survey "SG9309", based on well tops from well 7121/1-1 R.

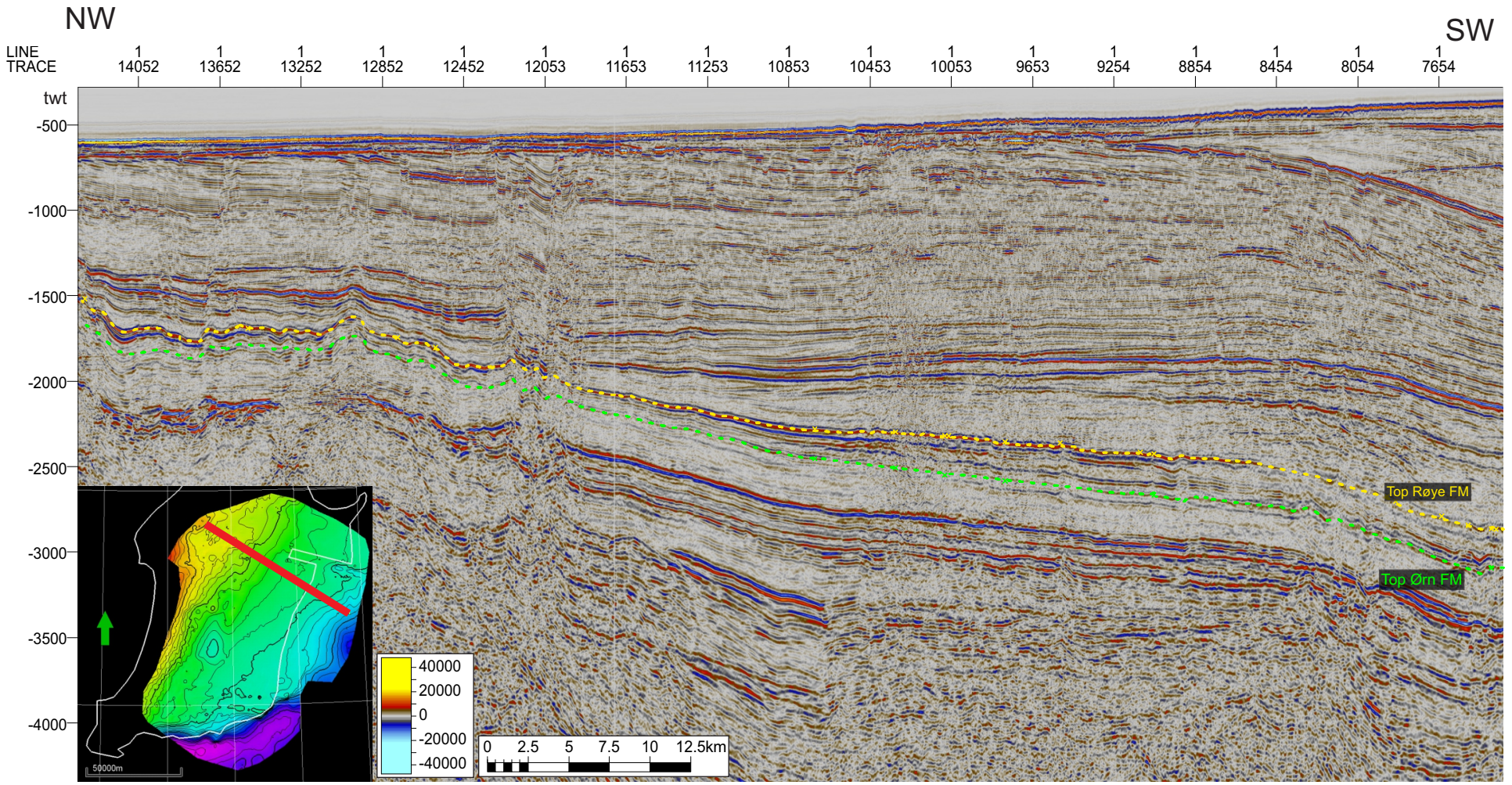

Fig. 4.3 Interpretation of Top Ørn and Top Røye on line D-6-85 from seismic survey "NPD-NOLO-85".

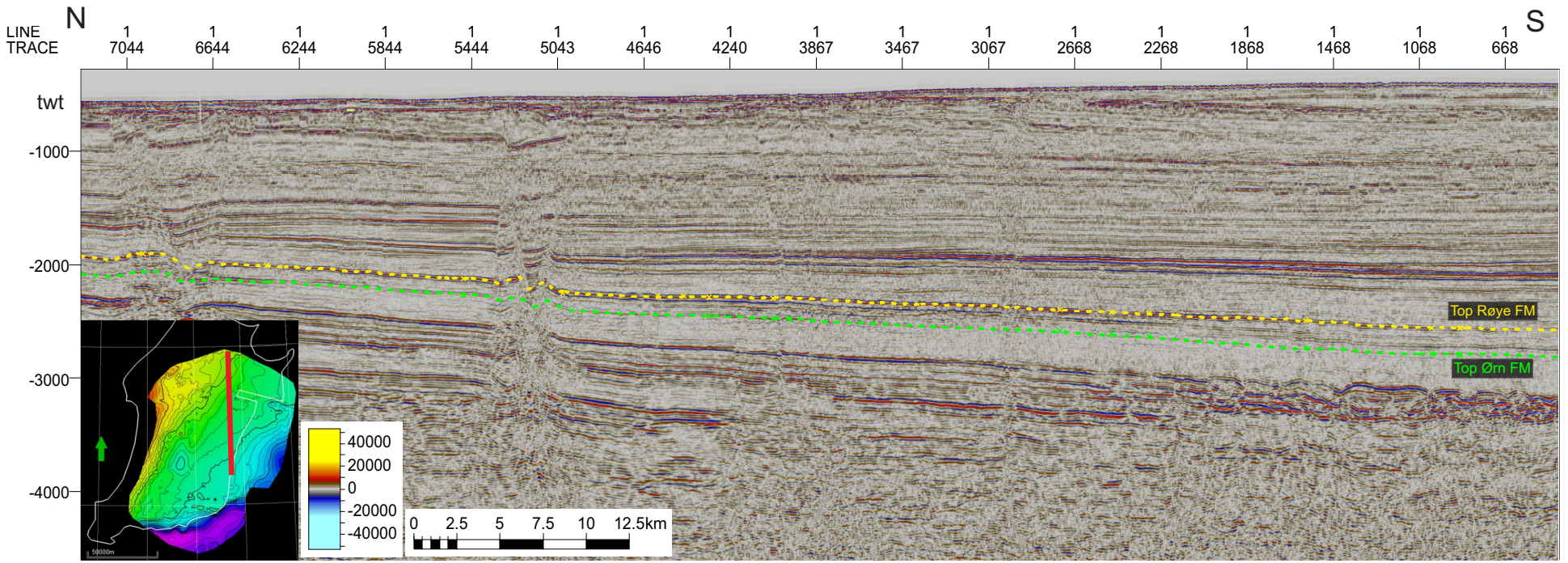

Fig. 4.4 Interpretation of Top Ørn and Top Røye on line 2245-85 from seismic survey "NPD-NOLO-85".

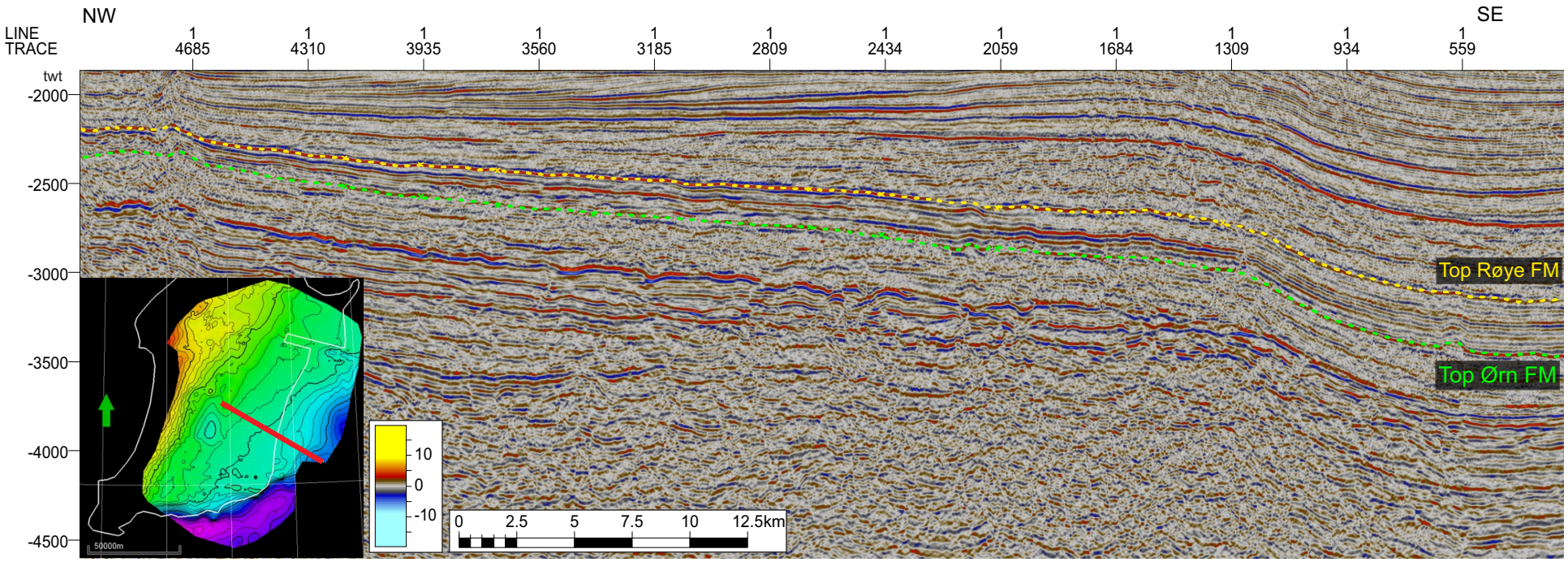

Fig. 4.5 Interpretation of Top Ørn and Top Røye on line 308 from seismic survey "ST8813".

The interpreted Top Ørn horizon is a NW-SE tilted horizon (Fig. 4.6), where the shallowest area in the NW is the location of the truncation of Top Ørn, and the deepest area in the SE is the drop after exiting the Loppa High boundary. The basin located west on the surface is a result of lack of data, Fig. 3.1 shows how the central area of Loppa High has no seismic coverage and this basin is presumably not present.

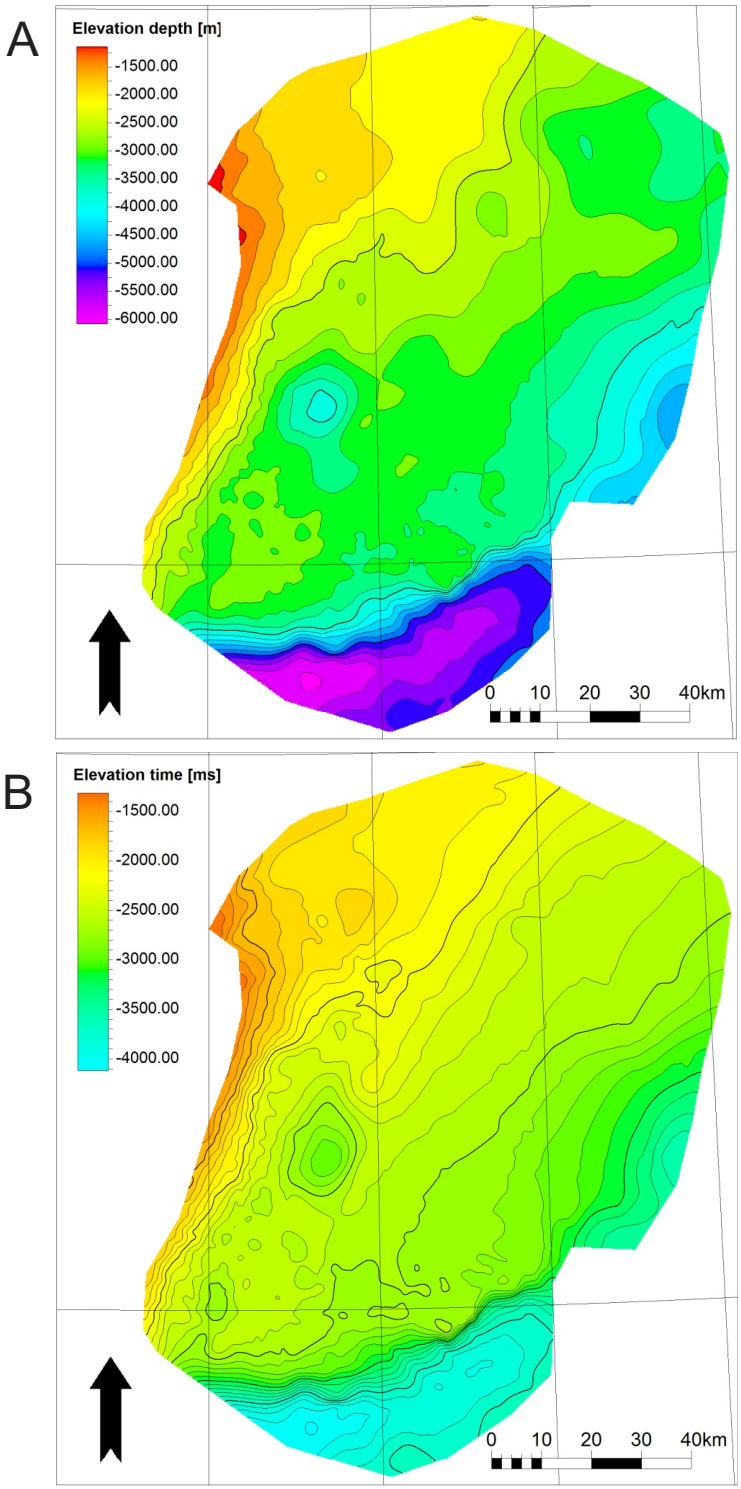

Fig. 4.6 A: Top Ørn surface converted to depth in meters (Countour intervals are 250m). B: Top Ørn surface in twt (Countour intervals are 100ms).

4.1.2 Top Røye FM

The potential source rock in the Palaeozoic interval in the Loppa High area is assumed to be the Permian interval where top Røye FM defines its top (<broken cross-reference>).

The interpretations are based on well tops from well 7121/1-1 R (NPD, 1986) and 7124/3-1 (NPD, 1987). The top Røye reflector is a peak with a high amplitude compared to its surrounding reflectors, and it is a relatively easy reflector to follow. However, in certain areas the seismic quality made the reflector hard to distinguish.

Well 7121/1-1 R is the key-well for the interpretations of Top Røye FM, this well is located in the south-eastern part of Loppa High. Line 102 from the seismic survey "SG-8737-Barents Sea" (Fig. 4.1) includes well 7121/1-1 R and shows the origin of the interpretation. This seismic line also shows the western termination of the Top Røye reflector in terms of a truncation. This truncation is present on the entire western part of the interpretations and can be seen in a north-south perspective on Fig. 4.2. Line 305 in the seismic survey "SG9309" (Fig. 4.2) shows the same dipping trend for Top Røye as Top Ørn, where the shallowest part is in the south. The dip is not only in south-north direction, it is also present west-east (Fig. 4.3) making the general dip southwest-northeast. The high in the north-west was faulted for the Top Ørn horizon and the same fault affects the shallower Top Røye horizon, further east the faulting stops and the smooth dip continues.

The central-eastern parts of the interpreted Top Røye horizon has a smooth dip with a steady angle from north to south (Fig. 4.4), the only interruption is two faults in the northern area. Line 408 from survey "ST8813" (Fig. 4.5) shows a northwest-southeast profile in the central-eastern area, towards NW Top Røye is affected by altercations before it smooths out towards SE, around trace 1309 the dip increases and Top Røye drops down indicating the edge of the Loppa High boundary.

Top Røye FM is a tilted formation with the shallowest parts in the NW and the deepest parts in SE (Fig. 4.7). The surface is generally smooth but contains a few minor faults in the northern area and the dip in the southeast shows the edge of Loppa High. Top Ørn surface had a false basin present and the same false basin is present in the Top Røye surface.

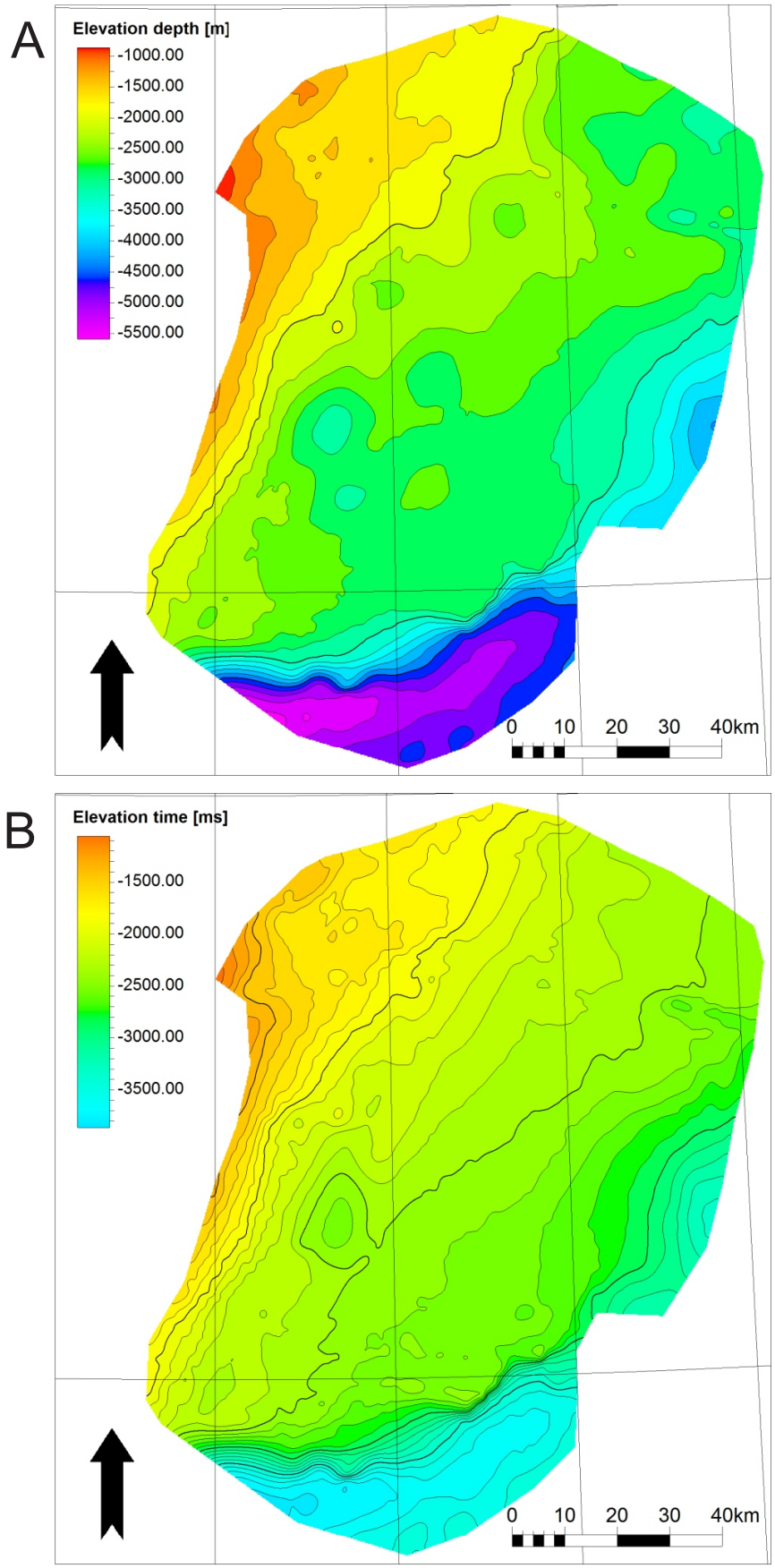

Fig. 4.7 A: Top Røye surface converted to depth in meters (Countour intervals are 250m). B: Top Røye surface in twt (Countour intervals are 100ms).

4.1.3 The Interpreted source-rock

The thickness of the interpreted source-rock is mostly ranging between 150m and 300m (Fig. 4.8), with a maximum thickness of 700m and minimum thickness of 0m. It is important to remember the lack of seismic in the central area where the "basin" is located, this basin (with thickness above 600m) is in a area with no seismic and should be seen as highly uncertain. The shallow area (thickness less than 200m) going from the "false basin" to the north-eastern edge where the thickness is 0m, is also affected by lack of seismic and the true thickness here is likely to be between 200-300m.

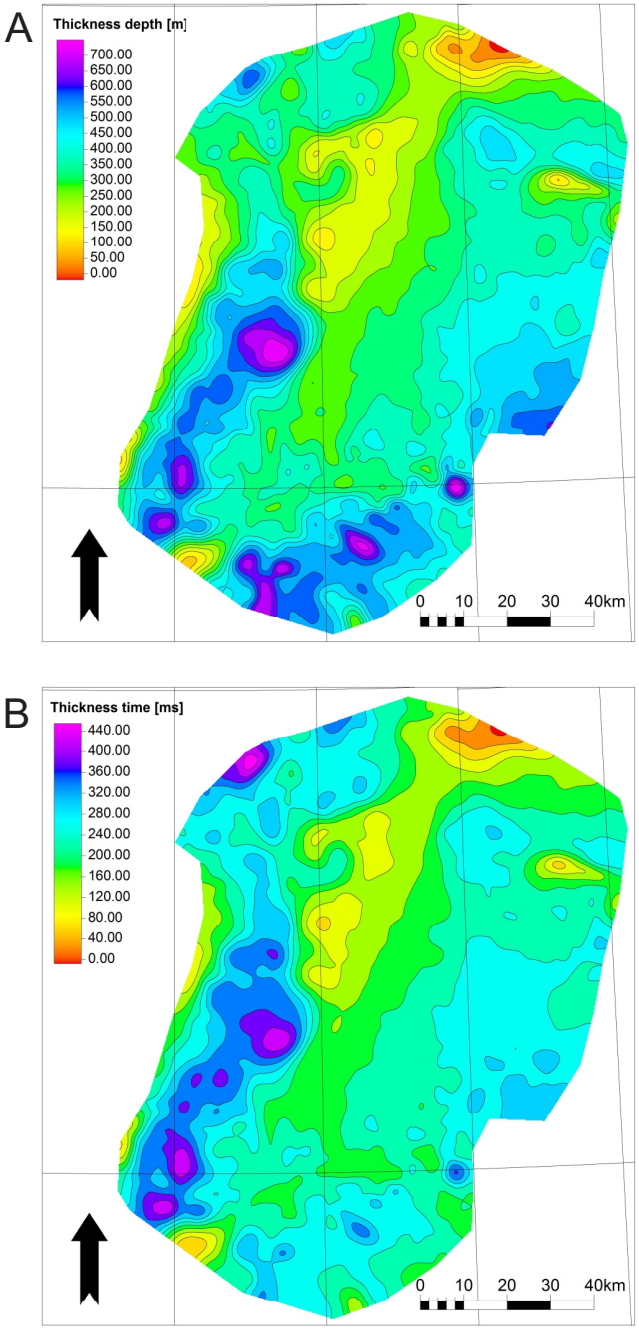

Fig. 4.8 Thickness map between Top Røye FM and Top Ørn FM. A: Thickness map in meters (Countour intervals are 50m). B: Thickness map in twt (Countour intervals are 40ms).

Before the PSQL modelling could be carried out the Palaeozoic depth of the source had to be accounted for. Henriksens map (Fig. 2.6) was geo-referenced in Petrel where the contour lines was used to create an erosion surface (Fig. 4.9). This erosion-surface shows net erosion in the interpreted area and was used to push down the interpreted top and bottom of the source rock, meaning that the northernmost part of the source was pushed down 2000m, while the southernmost part was pushed down 1000m. The new depth of the source rock will be closer to maximum burial depth.

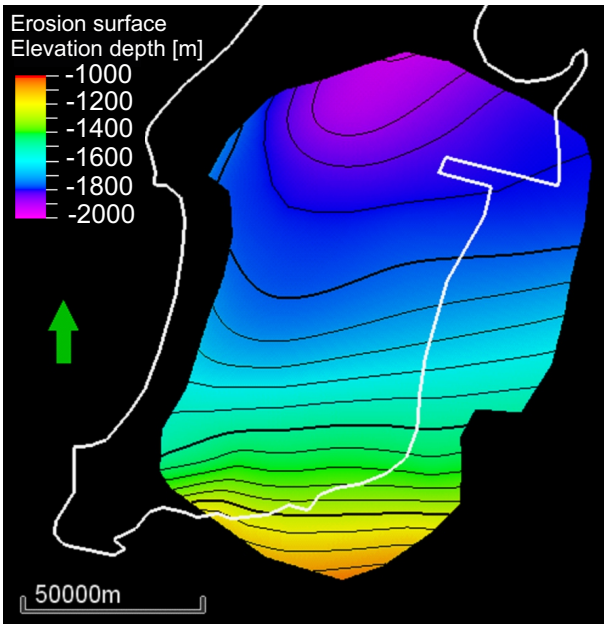

Fig. 4.9 Erosion surface.

4.2 PSQL modelling

4.2.1 P10 model

Temperature

The temperature model (Fig. 4.10A) uses a thermal gradient of 25°C and shows temperatures ranging from 60-115°C, where most of the source experience temperatures between 80-105°C. In the western and shallowest part of the source-rock the temperatures are between 70-80°C, while the central (and the biggest) area of the source rock has temperatures from 85-105°C. The deepest part of the source-rock, in the east-southeast shows temperatures from 110-115°C, these are the areas just outside of the Loppa High boundary and are significantly deeper then the rest of the source-rock. Temperatures above 70°C should be sufficient to let the source-rock enter the oil-window.

Vitrinite Reflectance

The vitrinite reflectance (Fig. 4.10B) ranges from 0.0-1.0 $\%R_o$, and the trend can be recognized from the temperature model. The shallow western parts of the source-rock shows values <0.55 $\%R_o$, which suggests that the oil generated here will be immature. The central and largest area of the source-rock shows a vitrinite reflectance between 0.5-0.7 $\%R_o$, which is the early oil window. The deepest part of the source-rock in the west-southwestern area shows a vitrinite reflectance between 0.7-1.0 $\%R_o$, this is the main oil window where we experience peak generation.

Bulk Transformation Ratio

The Bulk transformation ratio (Fig. 4.11A) is very stable for the central and western part of the source-rock and shows values <20%. In the deeper western parts the transformation ratio increases and consists of values from 30-50%.

Gas Generation Mass

The gas generation mass model (Fig. 4.11B) shows values ranging from 0-16'000 kg/m^2, whereas more than 90% of the source-rock shows values between 0 and 3000 kg/m^2. The only area with values above 3000 kg/m^2 is in the deeper eastern area. The total amount of gas generated is 2.91 billion kg/m^2.

Oil Generation Mass

The oil generation mass mass (Fig. 4.11C) shows values ranging from 0-650'000 kg/m^2, with more than 90% of the rock within the range of 0-150'000 kg/m^2, this area include the shallow western part and the big central area. The deep eastern part shows values from 150'000-650'000 kg/m^2. The total amount of oil generated is 143.78 billion kg/m^2.

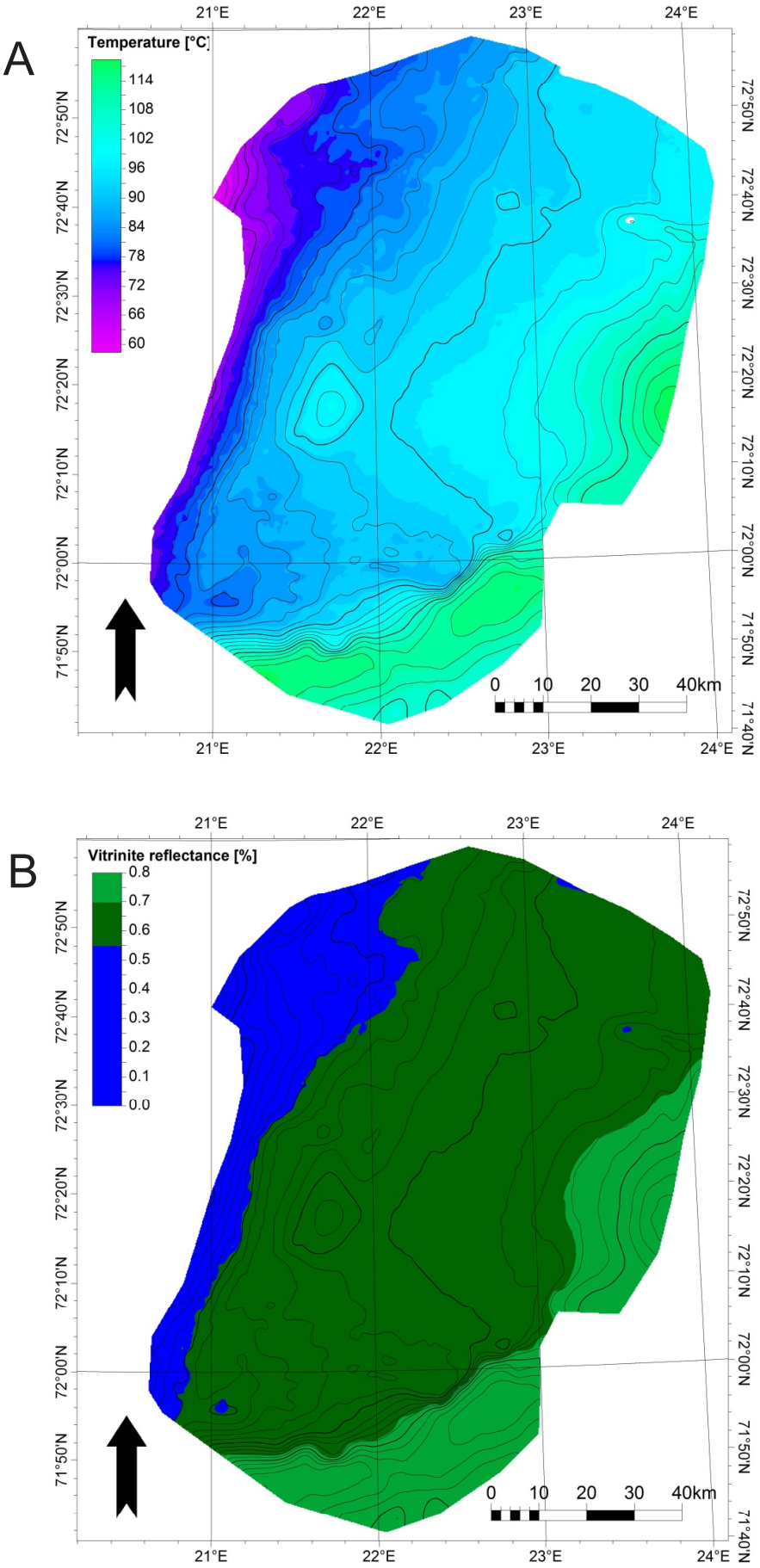

Fig. 4.10 A. Temperature surface for P10-model. B. Vitrinite reflectance surface for P10-model.

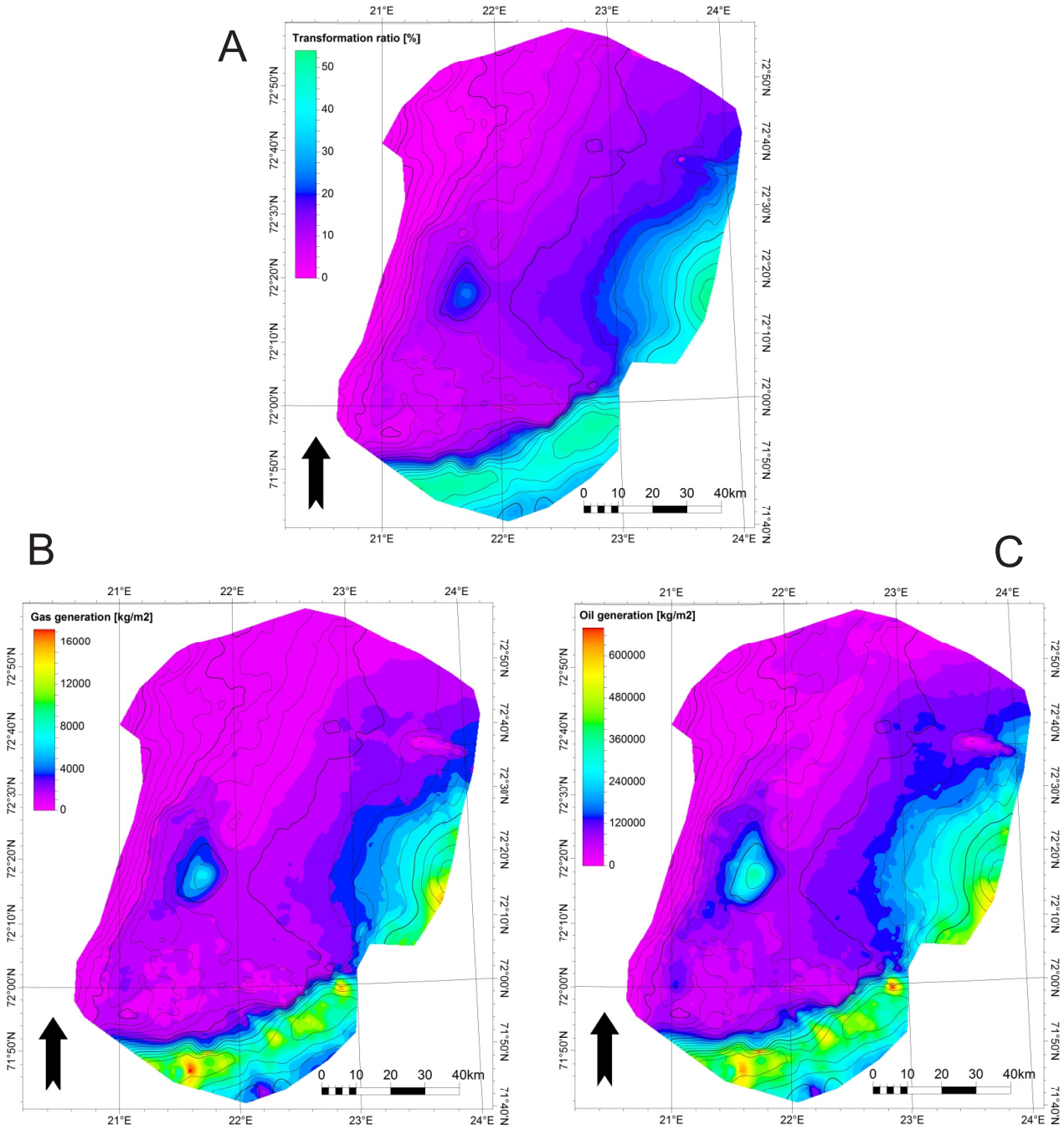

Fig. 4.11 A. Bulk transformation ratio from P10-model. B. Gas generation mass from P10-model. C. Oil generation mass from P10-model.

4.2.2 P50 model

Temperature

The temperature model (Fig. 4.12A) uses a thermal gradient of 30°C and shows temperatures ranging from 70-140°C, where most of the source-rock has temperatures ranging between 90-125° C. The shallow area in the west shows temperatures from 70-95°C, while the central and biggest area shows temperatures between 95-115°C. The deeper area in the east-southeast shows temperatures from 120-140°C.

Vitrinite Reflectance

The vitrinite reflectance model (Fig. 4.12B) gives values ranging from 0.0-1.1 $\%R_o$. In the shallow area in the vest has values from 0.0-0.7 $\%R_o$, leaving a small fraction of the source-rock in the "immature oil"-window. The central area of the source-rock shows vitrinite reflectance between 0.6-0.9 $\%R_o$, leaving it in the middle of the oil-generation window. In the deeper east-southeastern area the vitrinite reflectance ranges from 0.9-1.1 $\%R_o$, just above peak oil generation.

Bulk Transformation Ratio

The Bulk Transformation ratio (Fig. 4.13A) ranges from 0-85% and is >25% in the shallow western area. The central area has values from 25-50% while the deeper east-southeastern area has a transformation ratio between 50-85%.

Gas Generation Mass

The gas generation mass model (Fig. 4.13B) shows values ranging from 0-660'000 kg/m^2. The largest part of the source-rock, the western and central area combined, shows gas generation mass between 0-120'000 kg/m^2, while the deep east-southeastern part shows values from 240'000-660'000 kg/m^2. The total amount of gas generated is 73.68 billion kg/m^2.

Oil Generation Mass

The oil generation mass model (Fig. 4.13C) gives values ranging from 0-4'750'000 kg/m^2. The western and northern area have the lowest amount of generated oil with values from 0-1'000'000 kg/m^2. The central area have values from 1'000'000-2'500'000 kg/m^2, and the east-southeastern area have mainly values ranging from 2'750'000-4'000'000 kg/m^2. The total amount of oil generated is 1.56 trillion kg/m^2.

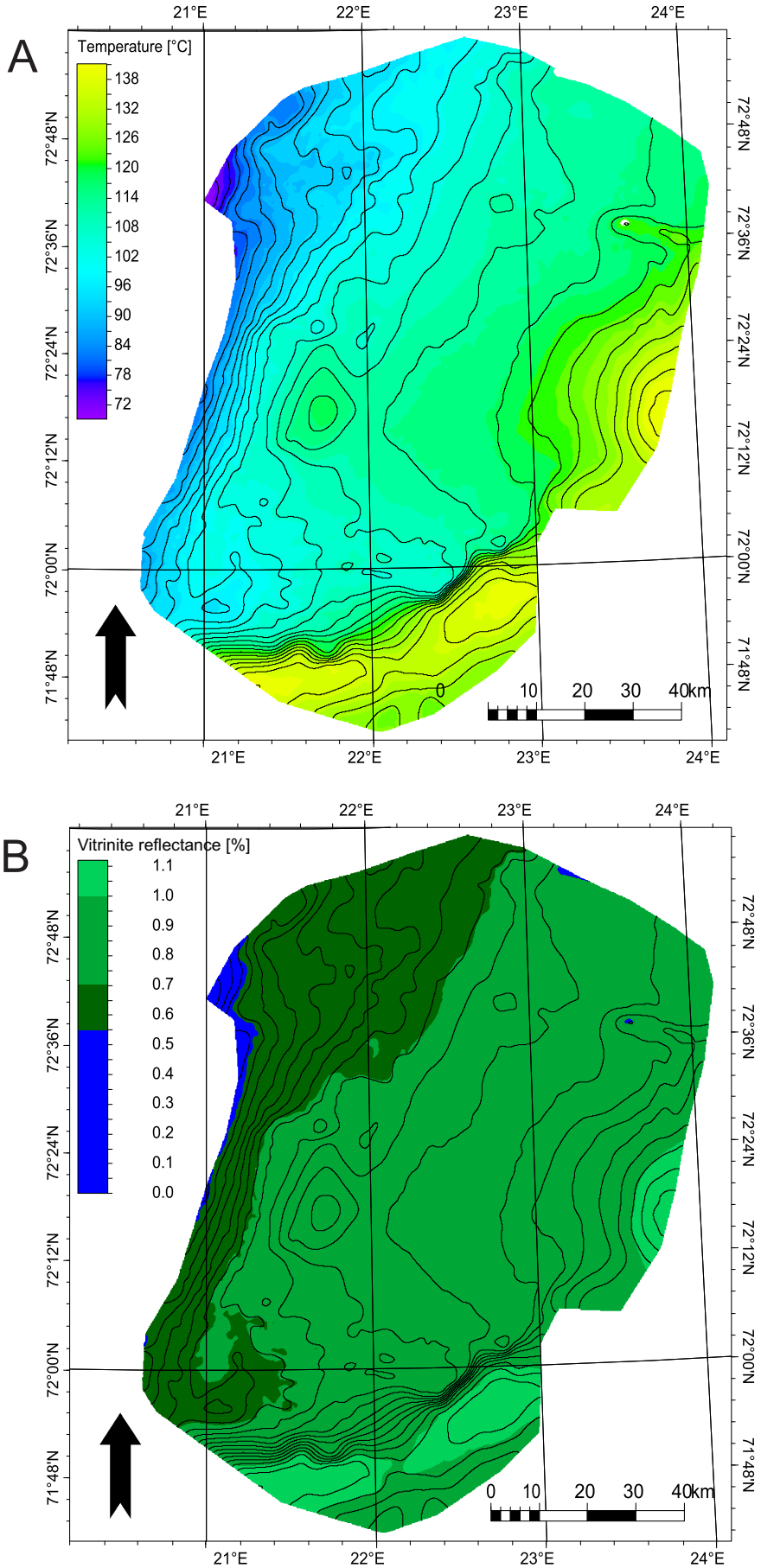

Fig. 4.12 A. Temperature surface for P50-model. B. Vitrinite reflectance surface for P50-model.

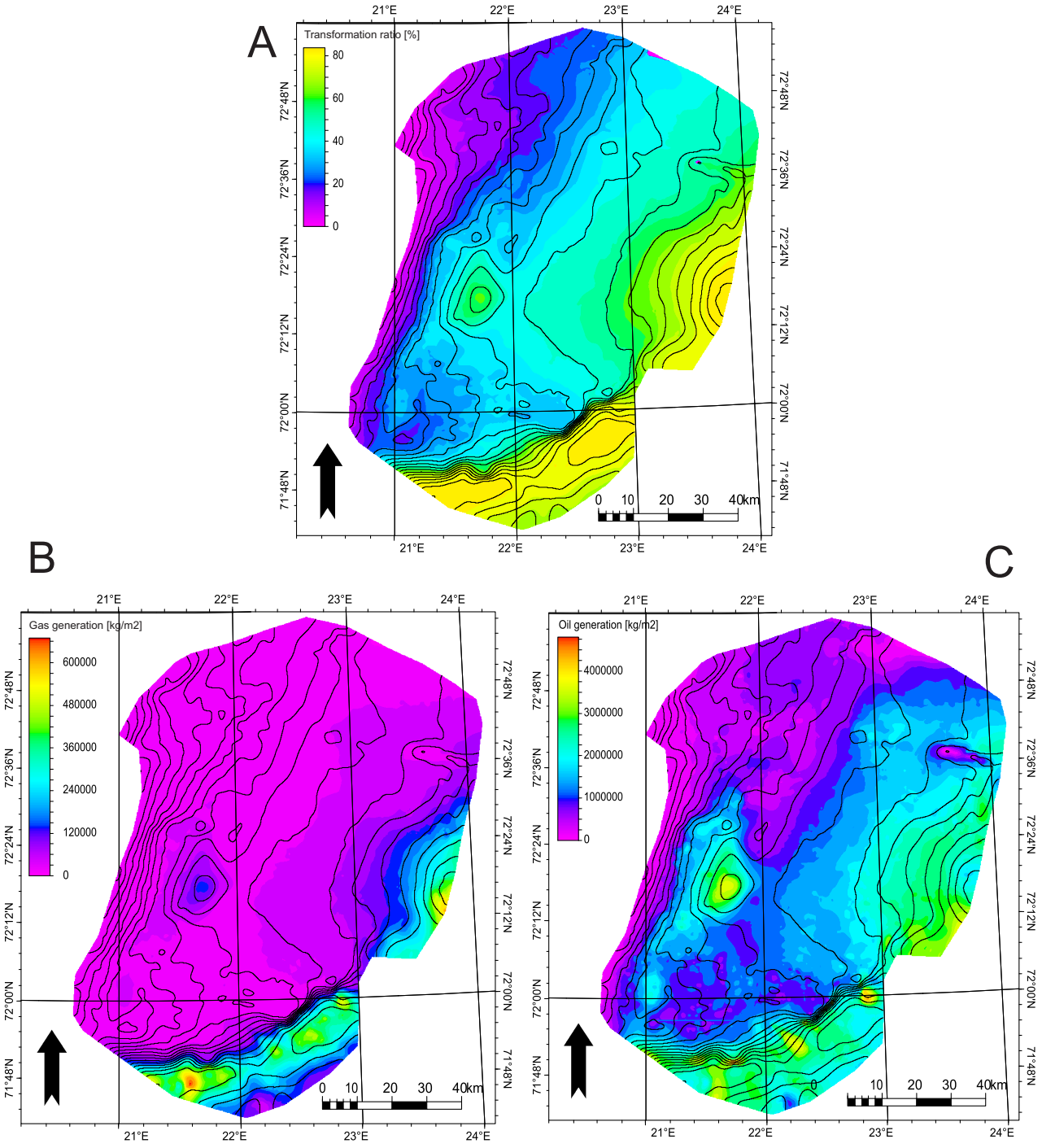

Fig. 4.13 A. Bulk transformation ratio from P50-model. B. Gas generation mass from P50-model. C. Oil generation mass from P50-model.

4.2.3 P90 model

Temperature

The temperature model (Fig. 4.14A) uses a thermal gradient of 35°C and gives temperatures ranging from 80-165°C, most of the source-rock is within a temperature-window of 100-150°C. The shallow western area have temperatures ranging from 80°C to 100°C, while the central parts gives temperatures from 115°C to 140°C. The deeper east-southeastern area gives temperatures from 150°C to 165°C.

Vitrinite Reflectance

The vitrinite reflectance (Fig. 4.14B) ranges from 0.0-1.55 $\%R_o$, but more than 80% of the source-rock has a vitrinite reflectance between 0.6 $\%R_o$ and 1.3 $\%R_o$. The shallow western area have values between 0.55 $\%R_o$ to 0.8 $\%R_o$, the central area have values from 0.8 $\%R_o$ to 1.1 $\%R_o$ and the deep east-southeastern area have values from 1.1 $\%R_o$ to 1.55 $\%R_o$.

Bulk Transformation Ratio

The bulk transformation ratio (Fig. 4.15A) is between 5% and 40% in the west, the central area have a transformation ratio ranging from 40% to 80% and the east-southeastern area have values ranging from 85% to 95%.

Gas Generation Mass

The gas generation mass model (Fig. 4.15B) ranges from 0-6'000'000 kg/m^2. The western, northern and central parts of the source-rock shows values from 0-1'200'000 kg/m^2, while the deep east-southeastern area contains the values from 2'400'000 kg/m^2 to 6'000'000 kg/m^2. The total amount of gas generated is 906.66 billion Sm^3.

Oil Generation Mass

The oil generation mass model (Fig. 4.15C) ranges from 0-12'000'000 kg/m^2. The western and northern area shows values from 0-4'000'000 kg/m^2, the central and eastern parts thats on top of the high shows values between 5'000'000 kg/m^2 and 9'000'000 kg/m^2. The total amount of oil generated is 4.1 trillion kg/m^2.

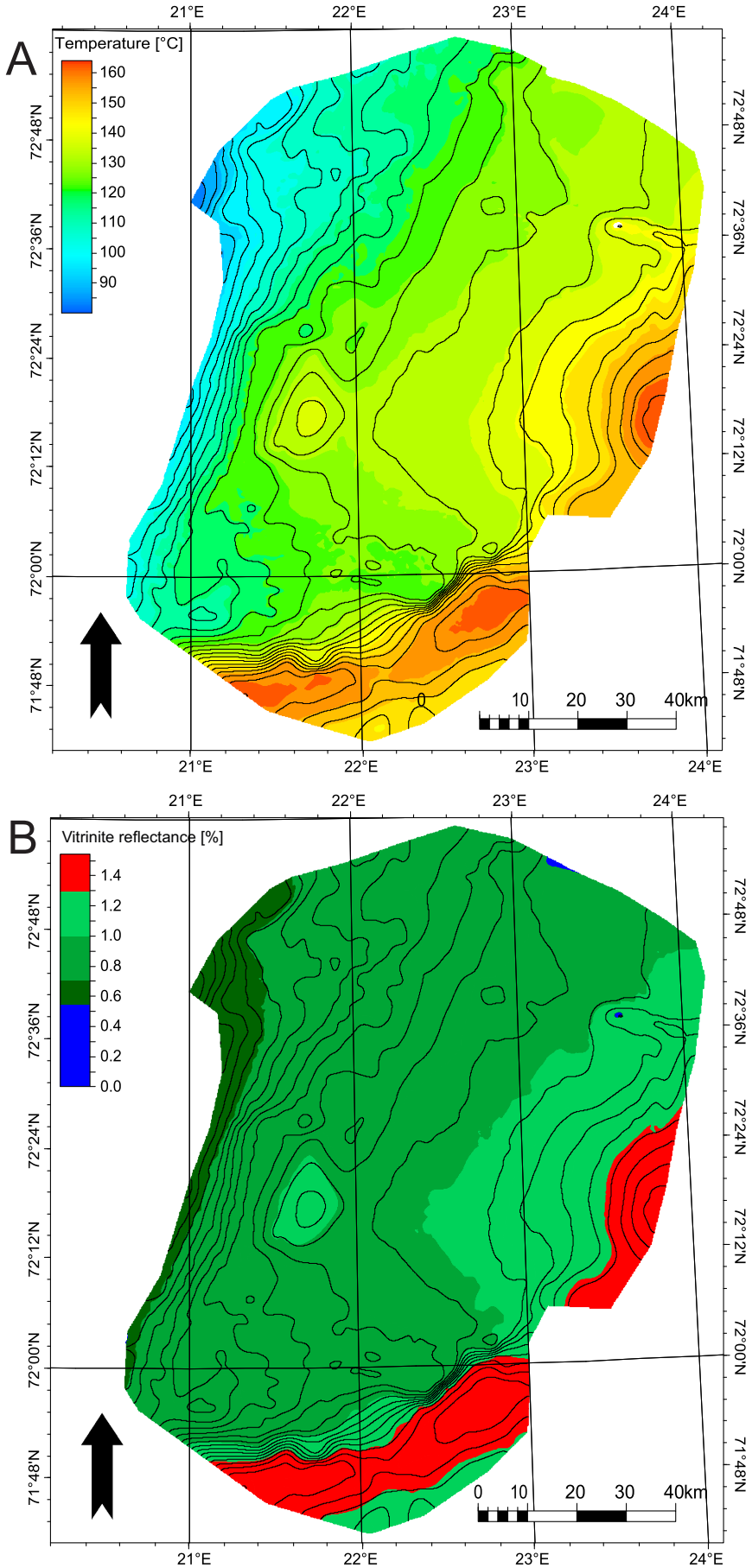

Fig. 4.14 A. Temperature surface for P90-model. B. Vitrinite reflectance surface for P90-model.

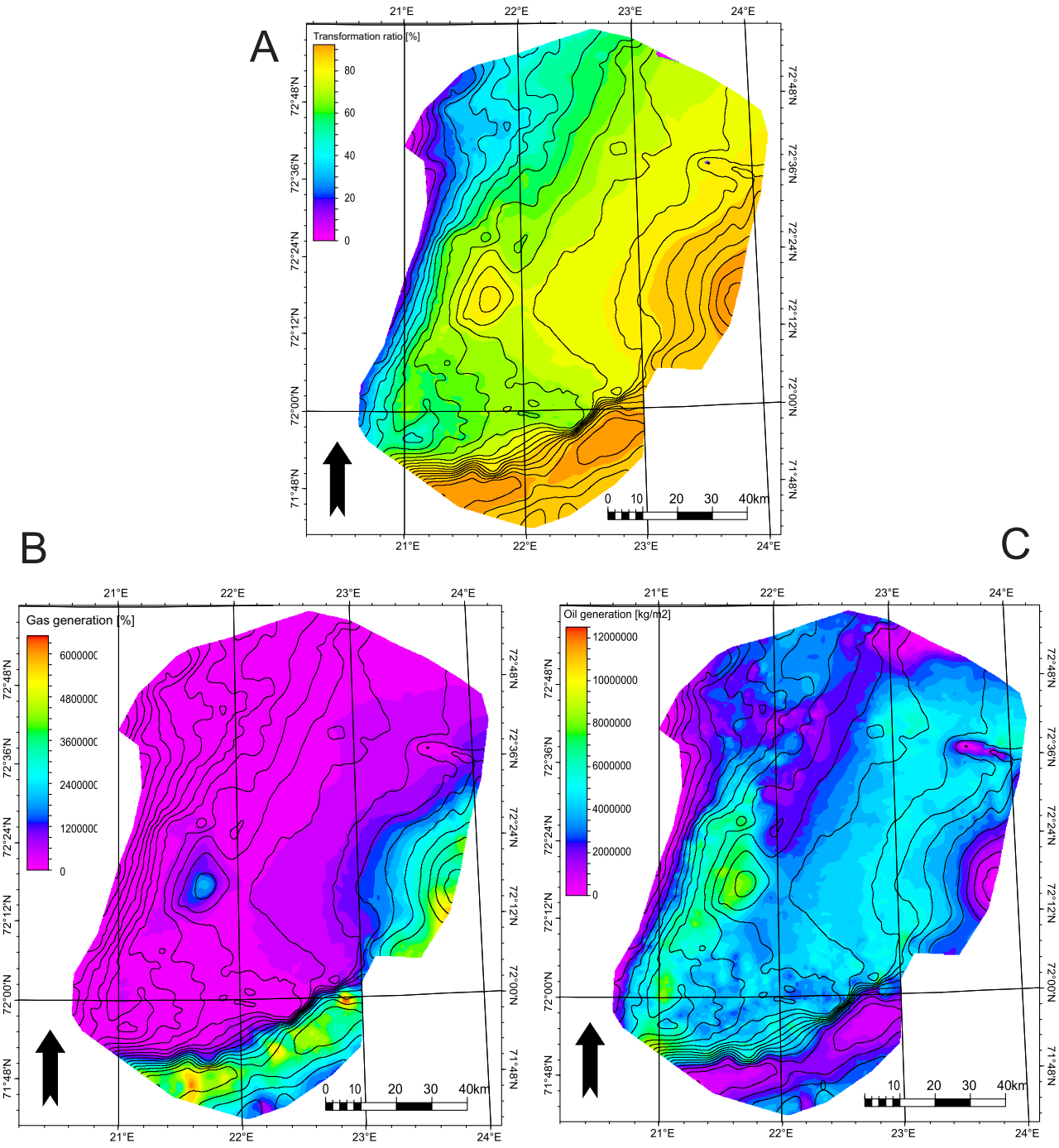

Fig. 4.15 A. Bulk transformation ratio from P90-model. B. Gas generation mass from P90-model. C. Oil generation mass from P90-model.

4.2.4 Hekkingen model

Temperature

The Hekkingen model (Fig. 4.16A) uses a thermal gradient of 30°C and shows temperatures ranging from 70-140°C. In the west temperatures ranges from 70-90°C, the central parts of the source-rock have temperatures from 90-120°C, and the east-southeastern area have temperatures between 120°C and 140°C.

Vitrinite Reflectance

The vitrinite reflectance model (Fig. 4.16B) gives values ranging from 0.9-1.1 $\%R_o$. In the western and northern area, values ranges from 0.0-0.7 $\%R_o$. In the central parts values ranges from 0.7-0.9 $\%R_o$ and in the east-southeastern parts the value ranges from 0.9-1.1 $\%R_o$.

Bulk Transformation Ratio

The bulk transformation ratio (Fig. 4.17A) ranges between 0-85%. In the north-western part of the source the ratio ranges from 5-25%, in the central area the ratio ranges from 25-50% and in the southeast the ratio ranges from 50-85%.

Gas Generation Mass

The gas generation mass (Fig. 4.17B) ranges from 0-8'750'000 kg/m^2. The western, northern and central parts of the source-rock shows values ranging from 0-2'000'000 kg/m^2 while the south-eastern area have vales from 2'000'000-8'750'000 kg/m^2. The total amount of gas generated is 1.07 trillion kg/m^2.

Oil Generation Mass

The oil generation mass (Fig. 4.17C) ranges from 0-69'000'000 kg/m^2. The western and northern area have values from 0-15'000'000 kg/m^2, the southern- and eastern-central part of the source-rock have values between 15'000'000-30'000'000. The east-southeasern area have generation values from 30'000'000-69'000'000 kg/m^2. The total amount of oil generated is 22.63 trillion kg/m^2.

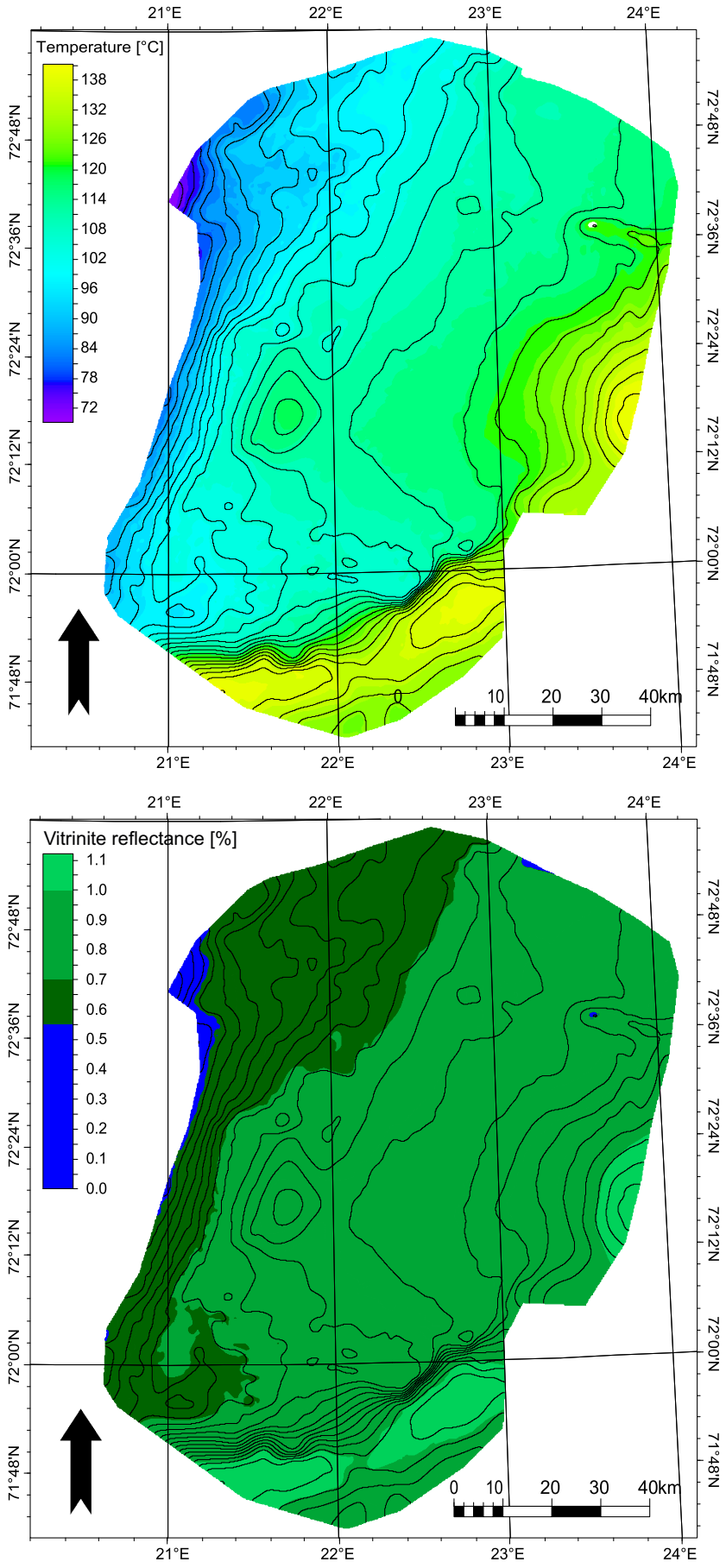

Fig. 4.16 A. Temperature surface for Hekkingen-model. B. Vitrinite reflectance surface for Hekkingen-model.

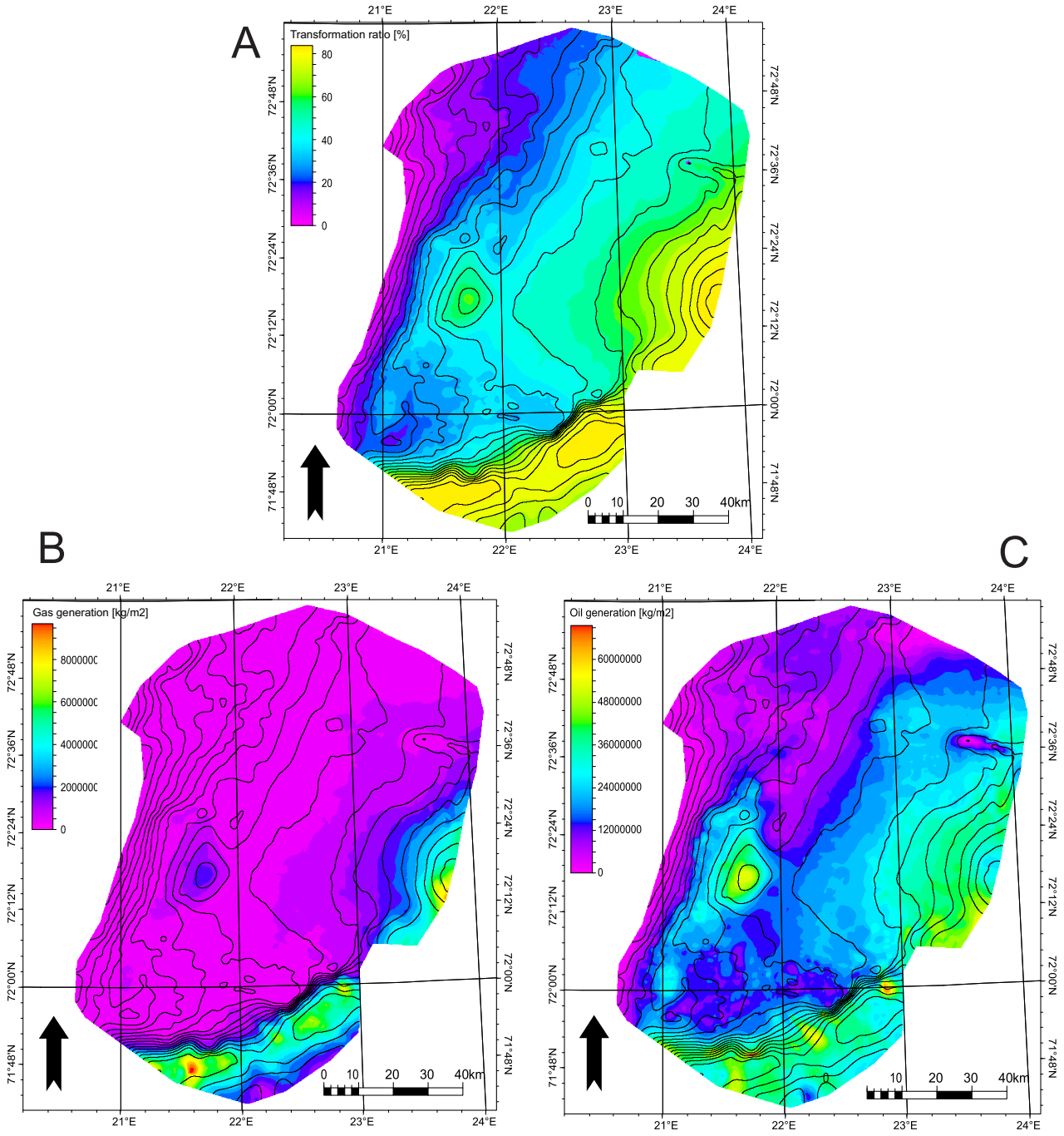

Fig. 4.17 A. Bulk transformation ratio from Hekkingen-model. B. Gas generation mass from Hekkingen-model. C. Oil generation mass from Hekkingen-model.

4.3 Oil and gas generation potential

27 of 30 models (excluding Hekkingen-model and the ±150m models) can be put into three categories based on their TOC-value; category A: 0.5% TOC (Fig. 4.18A & Fig. 4.19A), category B: 2.1% TOC (Fig. 4.18B & Fig. 4.19B) and category C: 3.5% TOC (Fig. 4.18C & Fig. 4.20C). The Hekkingen-model was created to get a perspective of how big the HC generation potential of the P10, P50 and P90-models are, for both oil generation (Fig. 4.20A) and gas generation (Fig. 4.20B).

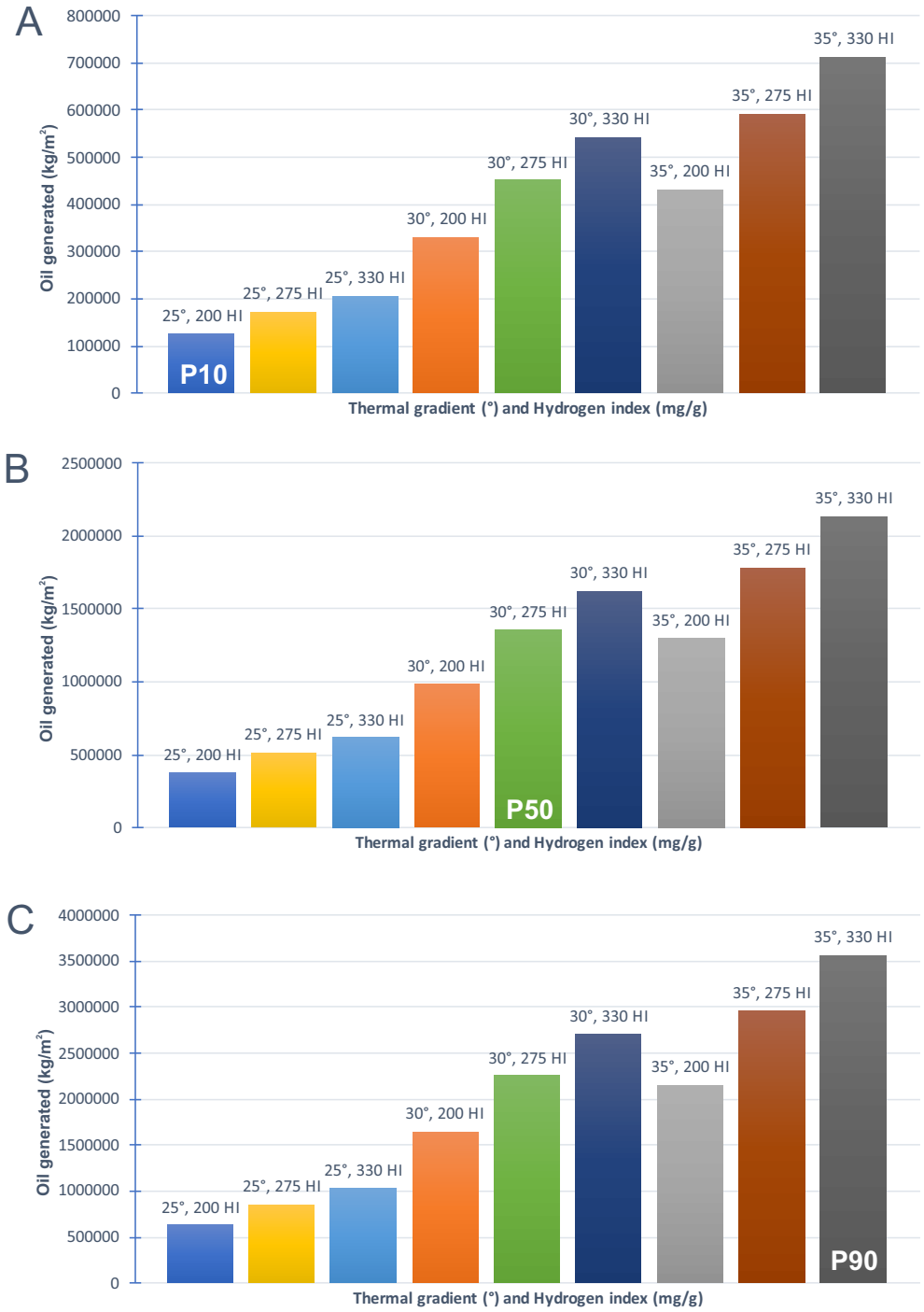

Fig. 4.18 Relative variation in oil generated for all the different models. A. TOC: 0.7%. B. TOC: 2.1%. C. TOC: 3.5%. Note: The "oil generated"-values shown are the average generation for the respective models.

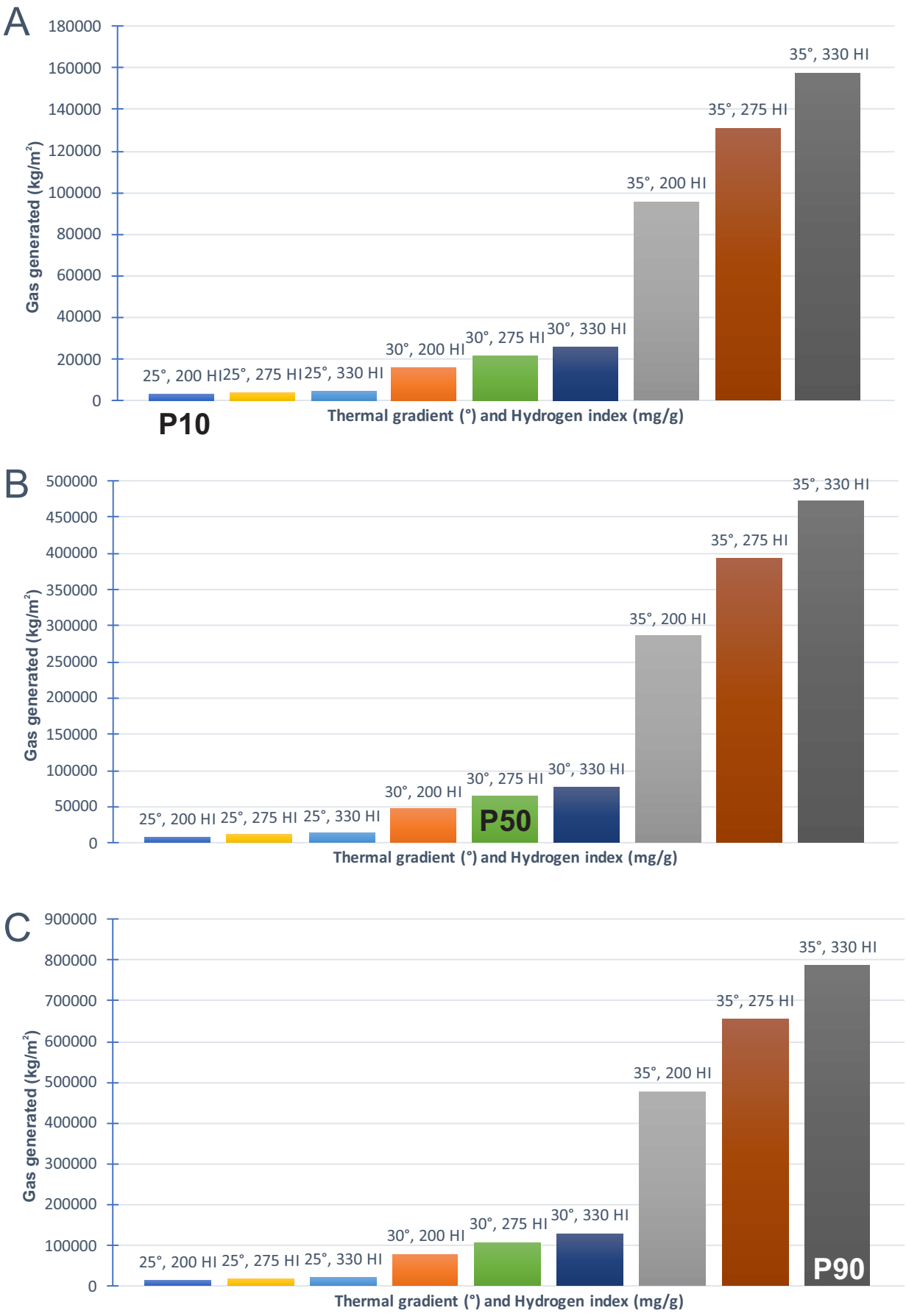

Fig. 4.19 Relative variation in gas generated for all models. A. TOC: 0.7%. B. TOC: 2.1%. C. TOC: 3.5%.
Note: The "gas generated"-values shown are the average generation for the respective models.

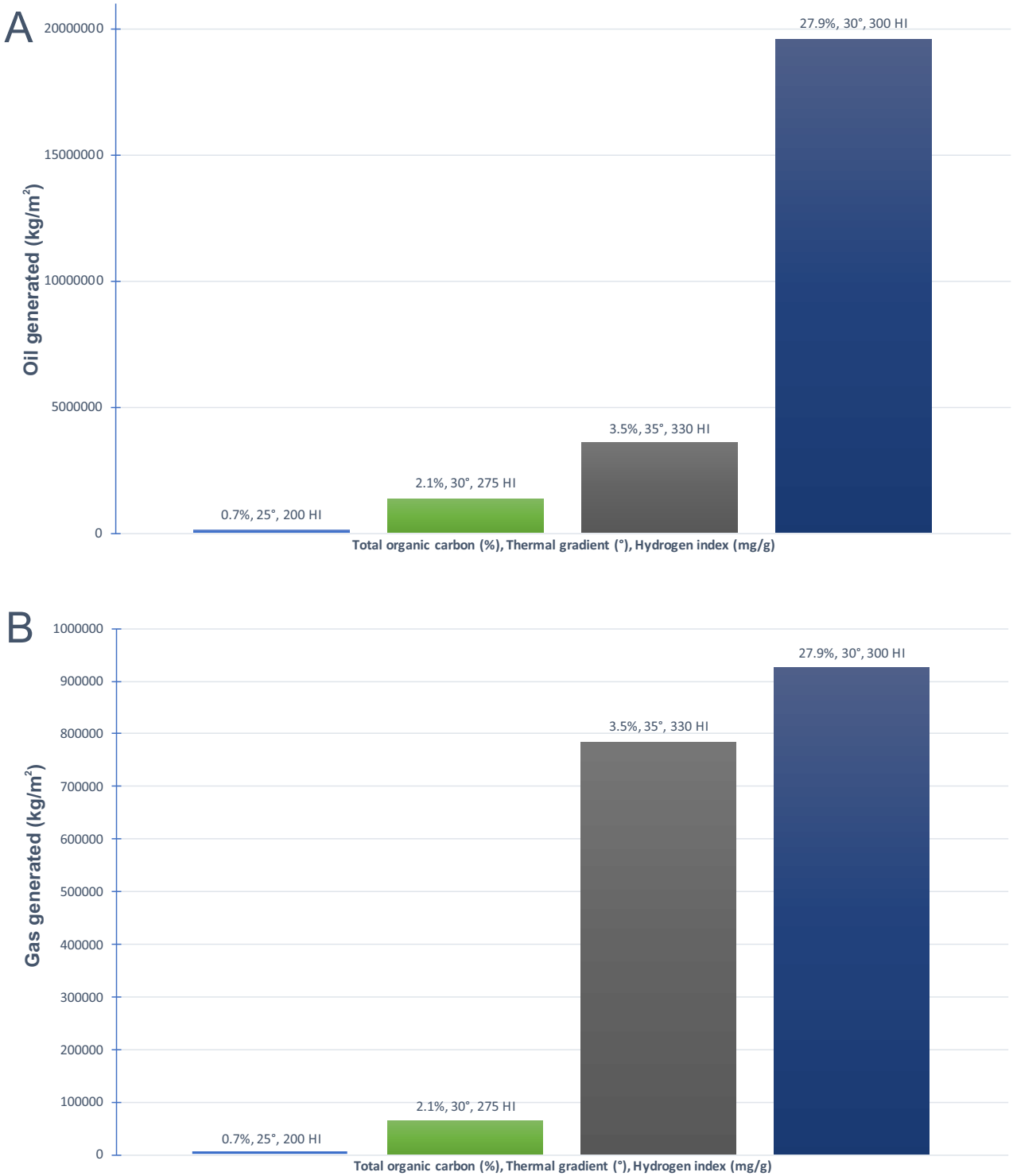

Fig. 4.20 A. Oil generated for P10, P50, P90 and Hekkingen model. B. Gas generated for P10, P50, P90 and Hekkingen model. Note: The "oil and gas generated"-values shown are the average generation for the respective models.

5 Discussion

The discussing will go through the key points of the interpreted source rock and how its sources of error will affect the PSQL-modelling. There will also be a discussion around the generation potential of the Palaeozoic interval in the Loppa High area based on all 30 models. Lastly the data will be compared to a recent study publish by the University of Oslo.

5.1 The source rock

The central parts of the interpreted source rock is highly affected by the lack of available 2D seismic in the area (Fig. 3.1) , and as a result Petrel have generated several basins, especially in the central-western area where the thickness is over 700m (Fig. 4.8). It is not possible with the available data to determine that this is wrong, but there are no signs on the seismic nearby that suggests the basins are actually present. Another inaccuracy regarding the source rock is the shallow area stretching north-east from the "fake basins", this area have a thickness from 0-120m which likely is a underestimation, this occurs due to low interpretation density giving Petrel a lot of freedom to grid the surface as it pleases.

There are several ways to fix this inaccuracy regarding the source rock, e.g. one can interpret more seismic lines and give Petrel less freedom. But in a basin modelling study the most important thing the thickness affects, is the total HC generation potential which is not the main focus in this study.

The well coverage for this study was also poor, while all four key-wells (Table 3.2) shows Top Ørn FM only two (well 7120/1-1 and 7121/1-1 R) shows Top Røye. The result of this is a highly uncertain interpretation for all areas except the south-western (where the key wells are located).

Although the source rock is full of uncertainties it should be a good starting point to determine if the Palaeozoic interval can be a potential source rock for the SW Barents Sea.

5.2 Source rock potential

There are two important details regarding the figures; firstly, the scales are heavily shifting for the Oil- and Gas generation surfaces (ranging from 0-10'000 kg/m^2 to 0-100'000'000 kg/m^2), so the colour on a specific surface will not be in relation to other surfaces showing the same type of data. Second, the term used in generation models are [kg/m^2] - this is a result of the PSQL-tools inability to calculate volumes, this will in turn make the total generation capability of the source-rock hard to determine, but the results will still be able to show the relative change of the system when the input values are altered.

5.2.1 P10 model

The P10 model uses the lowest amount of TOC (0.7%), has the lowest temperature gradient (25°C) and the lowest HI (200) of all the models. Still, the average TOC for a carbonate source rock is 0.7% (Chinn 1991) so the low amount of organic material should not stand in the way of generating HC's.

The vitrinite reflectance (Fig. 4.10B) shows that more than 2/3 of the potential source rock have entered the oil window, but 2/3 of the source rock has a bulk transformation ratio (Fig. 4.11A) below 20% resulting in a relative low amount of generated gas (Fig. 4.11B) and oil (Fig. 4.11C), most likely due to the low temperature in this area (Fig. 4.10A).

When comparing the P10-models' generated HC's to the proven Hekkingen source rock (Fig. 4.20A) it is clear that the generation potential is low, and that the P10-model likely would not work as a viable source rock.

5.2.2 P50 model

The P50 model is the average model which uses the input values most likely to represent the true values. Its TOC is 2.1%, the temperature gradient is 30°C and the HI is 275.

Almost the entire source rock is within the oil window (Fig. 4.12B), 1/3 is in the early oil window while the rest is in the main oil. Only a slight portion in the deep south-eastern area is in the late oil window. With the source rock well within the oil window the generation potential should be good, the bulk transformation ratio is varying, but more than 50% of the source rock have a bulk transformation ratio above 40%, which means that a good portion of the TOC have transformed into HC's.

When first looking at the gas and oil generation (Fig. 4.13B & C) it looks like the generation potential is low, at least for the gas model, but when comparing the generation values in the P50 model to the P10 model it is obvious that the potential in the P50 model is significantly higher. The big western area with the uniform colour code on Fig. 4.14B indicates that the values are on the lower range of the scale, but it is still up to 120'000 kg/m^2, whereas the maximum values on the P10 gas generation model were 10'000 kg/m^2.

The erosion-correction that was carried out on the interpreted source rock had an uncertainty of ±150m, so two extra models was made to see how much ±150m would affect the source potential. The input value that was used was identical to the P50 model, only the source rock was pushed down/up 150m. The resulting change in generation potential (Fig. 5.1) was not very significant. When the source rock was 150m deeper the increase in oil generated (P50: 1.35 million kg/m^2 vs. 150m deeper: 1.55 million kg/m^2) was smaller than when the only change on the model was 275 HI (P50) to 330 HI (1.62 million kg/m^2). The increase in gas generation was bigger than the increase in oil generation, this is likely due to the fact that temperature is the factor that increases most when the source rock is pushed deeper.

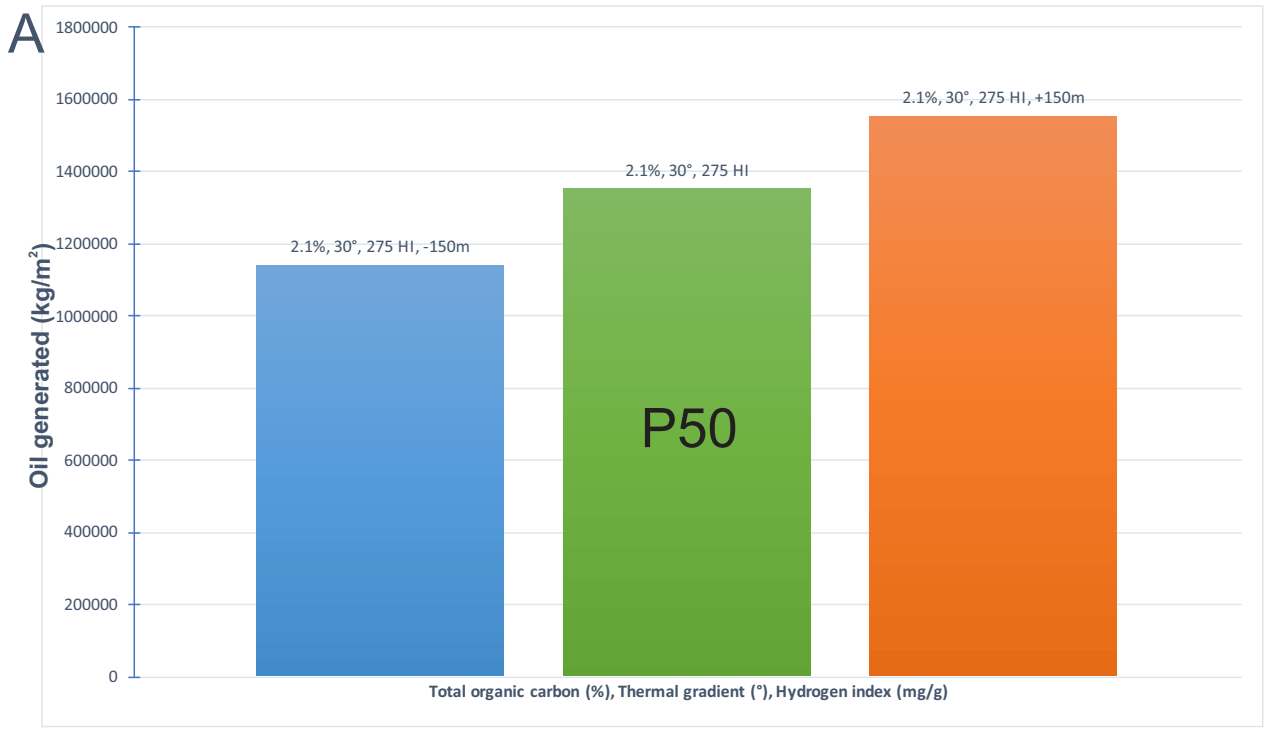

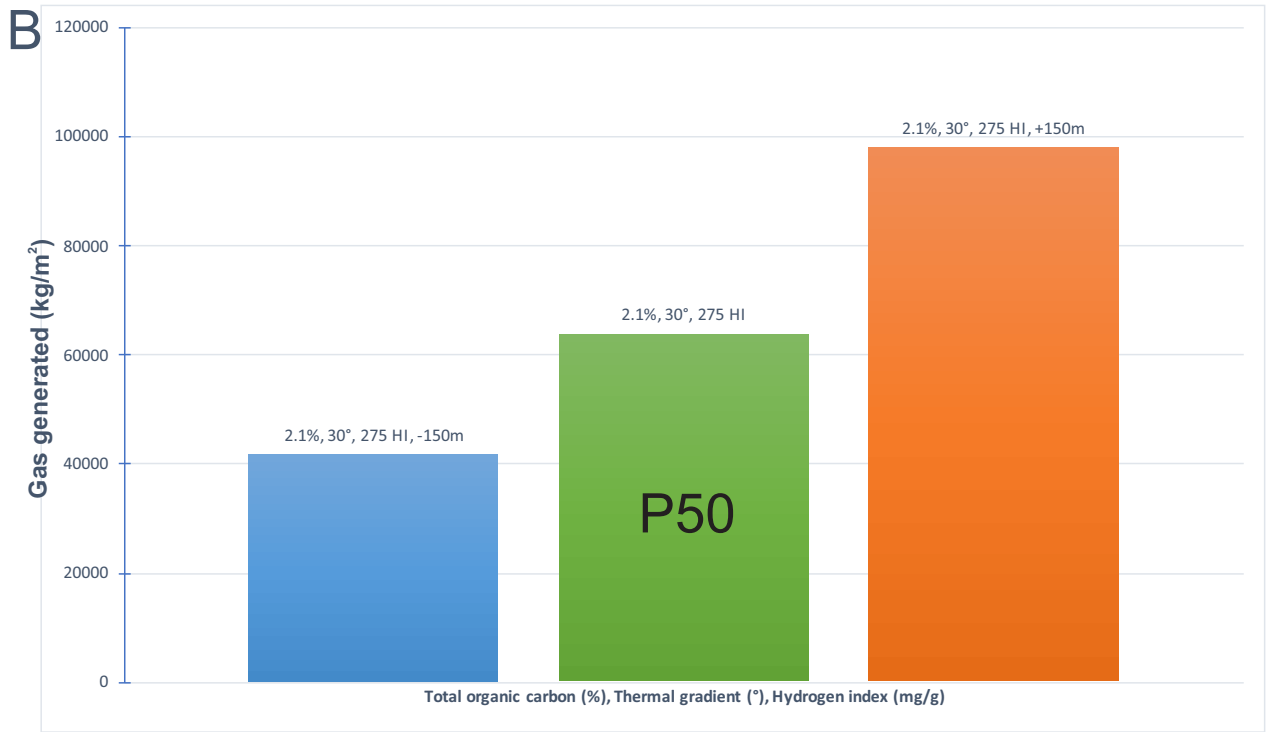

Fig. 5.1 A. Average oil generated for P50 model with 150m less erosion (blue), P50 model (green), and P50 with 150m more erosion (orange), respectively. B. Average gas generated for P50 model with 150m less erosion, P50 model, and P50 with 150m more erosion, respectively.

5.2.3 P90 model

The P90 model is the maximum model, and uses all the highest values used in this thesis; its TOC is 3.5%, the temperature gradient is 35°C and the hydrogen index is 330.

Only a small fraction of the source rock is in the early oil window (Fig. 4.14B), the rest of the source is in the main and late oil window with a small portion of the deepest parts entering the wet gas window. The bulk transformation ratio (Fig. 4.15A) is also significantly increasing, almost the entire source have a ratio above 40%, and around 50% of the source rock have a ratio above 80%.

The amount of HC's produced in this model is significantly higher than P10 and P50, which is to be expected. The oil generation (Fig. 4.20C) is not biggest in the deepest parts of the source, which it is for the P10 and P50 model, this means that the temperature puts the central parts of this source rock in the middle of peak oil generation. The increase in amount of average generated oil for the P90 model, when compared to the two other highlighted models, is not as big as the increase in average gas generated (Fig. 4.20). The source potential in this model would be very good.

5.2.4 Hekkingen model

The only difference between the P50 model and the Hekkingen model is the TOC where the Hekkingen model uses 27.9%, so the Hekkingen models' surfaces are identical in terms of looks, but the values differ (from the P50 model). The total amount of HC’s generated in the Hekkingen model is, as expected, a lot higher than for the other models. The biggest increase is in average oil generated (Fig. 4.20A) where the P90 model only produces ~18% of what the Hekkingen model produces, for average gas generation the P90 model produces ~85% of what the Hekkingen model does.

5.2.5 All models

When looking at the average HC generation potential for all models (Fig. 4.18 & Fig. 4.19) some trends can be observed, at first look it is obvious that the increase in temperature significantly increases the generation potential - especially for gas. All models experience a significant increase in average gas generation from 30°C to 35°C, and the P90 model produced almost the same amount of gas as the Hekkingen model, this suggests that temperature gradient is the most important input-value for gas generation mass. The same is not the case for oil generation, here the P90 model only produced 18% of what the Hekkingen model does, suggesting that the biggest factor in oil generation is the TOC.

The increase in average oil and gas generation mass when increasing the TOC from 0.7% to 2.1% is 200% (for all models with the same thermal gradient and HI), and the increase when going from 2.1% to 3.5% TOC is 66%.

5.3 Other studies and potential further studies

A recent study by Matapour et al. from the University of Oslo (Matapour, 2017) concludes that the Alta and Gohta discoveries in the Loppa High contains oils with a Palaeozoic origin. Furthermore they present evidence that the Alta and Gohta oil represent blends of petroleum expelled at maturities ranging from 1.0 $\%R_o$ to just over 1.3 $\%R_o$. The maturity range on the P50 model in this study is mainly between 0.6 $\%R_o$ to 1.1 $\%R_o$ (Fig. 4.12B), while the P90 model has a maturity range mainly ranging from 0.8 $\%R_o$ to 1.3 $\%R_o$ (Fig. 4.14B).

The PSQL module consists of 4 steps (Fig. 3.6), and only one of them have been utilized in this study (modelling of the generation potential). It would be interesting to see if further use of the Petroleum System Quick Look tool could strengthen the theory that the interpreted Palaeozoic source rock is the source of the HC's found in Alta and Gohta.

6 Conclusion

- A Palaeozoic source rock with Top Ørn as bottom and Top Røye have been interpreted, furthermore a net-erosion correction was carried out ensuring that the potential source rock was closer to its historically deepest position.
- The basin modelling performed on the interpreted source rock have resulted in 30 unique models, showing how the potential source rock responds to changes in depth, thermal gradient, TOC and HI. 4 of the models are displayed with their resulting temperature surface, vitrinite reflectance surface, bulk transformation ratio surface, gas generation mass surface and oil generation mass surface. The other 26 models are shown in tables highlighting their average gas- and oil generation mass and how their generation potential is relative to each other.
- The interpreted source rock from the Palaeozoic interval in the Loppa High area should (from this study) be classified as a potential source rock - all 28 models have shown the ability to produce HC's albeit the P10 model produces very little.

7 References

Brown, A. R., (1999). *Interpretation of three-dimensional seismic data.* 5th edition. AAPG Memoir 42, pp. 514.

Basset, M. G. (2002). *Sub-Devonian geology.* In: The Millennium Atlas: petroleum geology of the central and northern North Sea. The Geological Society of London, pp. 61-63

Bugge, T., et al., (1995). *The Upper Palaeozoic succession on the Finnmark Platform, Barents Sea.* Norsk Geologisk Tidssskrift 75

Chinn, E. W., (1991). *The role of organic geochemistry in petroleum exploration.* Basin Research Institute Bulletin, Louisiana State University, Baton Rouge, LA, p. 15–23.

Doré, A. G., (1994). *Barents Sea geology, petroleum resources and commercial potential*. Arctic, v. 48, no. 3.

Dow, W. G., & Magoon, L. B., (1994). *The Petroleum System.* In: The petroleum system - from source to trap: AAPG Memoir *60*, Chapter 1, pp. 3-24.

Faleide, J. I., Gudlaugsson, S. T., & Jacquart, G., (1984). *Evolution of the western Barents Sea*. Department of Geology, University of Oslo.

Faleide, J. I., Vågnes, E., & Gudlaugsson, S. T., (1993). *Late Mesozoic-Cenozoic evolution of the south-western Barents Sea in a regional rift-shear tectonic setting.*

Gabrielsen, R. H., Faerseth, R. B., & Jensen, L. N., (1990). *Structural Elements of the Norwegian Continental Shelf.* Part 1. The Barents Sea Region. Norwegian Petroleum Directorate, Bulletin 6.

Gernigon, L., Brönner, M., Roberts, D., Olesen, O., Nasuti, A., & Yamasaki, T., (2013). *Crustal and basin evolution of the southwestern Barents Sea: From Caledonian orogeny to continental breakup.*

Glørstad-Clark, E., Faleide, J., Lundschien, B. & Nystuen, j., (2010). T*riassic seismic sequence stratigraphy and paleogeography of the western Barents Sea.* Marine and Petroleum Geology, Volume 27, pp. 1448-1475

Gudlaugsson, S. T., Faleide, J. I., Johansen, S. E., & Breivik., A. J., (1998). *Late Palaeozoic structural development of the South-Western Barents Sea.*

Halland, E. K., Bjørnestad, A., Gjeldvik, I. T., Bjørheim, M., Magnus, C., & Meling I. M., (2013). *CO2 storage atlas Barents Sea.* NPD, Chapter 4 Geological description of the Barents Sea.

Hantschel, T. & Kauerauf, A.I., (2009). *Fundamentals of Basin and Petroleum Systems Modeling.* Springer

Henriksen, E., Ryseth, A. E., Larssen, G. B., Heide, T., Rønning, K., Sollid, K., & Stoupakova, A. V., (2011a). *Tectonostratigraphy of the greater Barents Sea: implications for petroleum systems.* Geological Society, London, Memoirs 2011; v. 35; p. 163-195

Henriksen, E., Bjørnseth, H. M., Hals, T. K., Heide, T., Kiryukhina, T., Kløvjan, O. S., Larssen, G. B., Ryseth, A. E., Rønning, K., Sollid, K., & Stoupakova, A., (2011b). *Uplift and erosion of the greater Barents Sea: impact on prospectivity and petroleum systems.* Geological Society, London, Memoirs 2011; v. 35; p. 271-281

Jacobson, S. R., (1991). *Petroleum Source Rocks and Organic Facies.* In: Source and Migration Processes and Evaluation Techniques. United States. p. 8-11.

Khutorskoi, M. D., Viskunova, K. G., Podgornykh, L. V., Suprunenko, O. I., & Akhmedzyanov, V. R. (2008). *A Temperature Model of the Crust beneath the Barents Sea: Investigations along Geotraverses.* Geological Institute, Russian Academy of Sciences.

Larssen, G. B., Elvebakk, G., Henriksen, L. B., Kristensen, S.-E., Nilsson, I., Samuelsberg, T. A., Stemmerik, L., Worsely, D., (2002). *Upper Paleozoic lithostratigraphy of the southern Norwegian Barents Sea.* Norsk Geologisk Undersøkelser, Bulletin 444, 43. Geological Survey of Norway, Trondheim.

Mangerud, G., (1994). *Palynostratigraphy of the Permian and lowermost Triassic succession, Finnmark Platform, Barents Sea.* Review of Palaeobotany and Palynology

Matapour, Z., Karlsen, D. A., Lerch, B., & Backer-Owe K., (2017). *Petroleum occurrences in the carbonate lithologies of the Gohta and Alta discoveries in the Barents Sea, Arctic Norway.* Department of Geosciences, University of Oslo.

Ohm, S. e., Karlsen, D. A., Austin, T. J. F., (2008). *Geochemically driven exploration models in uplifted areas: Examples from the Norwegian Barents Sea.* AAPG Bulletin, v. 92, no. 9

Pedersen, J. H., Karlsen, D. A., Brunstad, H., Lie, J. E., (2006). *Source rocks of the Norwegian Barents Sea I.* Department of Geosciences, University of Oslo

Sayago, J., Di Lucia, M., Mutti, M., Cotti, A., Sitta, A., Broberg, K., Przybylo, A., Buonaguro, R., & Zimina, O., (2012). *Characterization of a deeply buried paleokarst terrain in the Loppa High using coredata and multi attribute seismic facies classification.* AAPG Bulletin, v. 96, no. 10.

Sheriff, R. E., (1985) *Aspects of Seismic Resolution.* In: Seismic Stratigraphy II: American Association of Petroleum Geologist, memoir, Volume 39, pp. 1-10.

Smelror, M., Petrov, O., Larssen, G. B., & Werner, S., (2009). *Geological history of the Barents Sea.* Norges Geol. undersøkelse, 1-135.

Thiessen, O., (2013). *Petroleum Systems of the Norwegian Barents Sea.* Search and Discovery Article #90177. 3P Arctic Conference & Exhibition. The Polar Petroleum Potential.

Tissot, B. P., & Welte, D. H., (1984). *Petroleum Formation and Occurrence,* 2 ed.: New York, Springer-Verlag, 699 p.

Wood, R. J., Edrich, S. P., & Hutchison, I., (1989). *Influence of North Atlantic Tectonics on the Large-Scale Uplift of the Stappen High and Loppa High, Western Barents Shelf*: Chapter 36: North Sea and Barents Shelf. AAPG, 559-566.

Waples, D. W. (1998). *Basin modelling: how well have we done?*. In: DUPPENBECKER, S. J. & ILIFFE, J. E. (eds) Basin Modelling: Practice and Progress. Geological Society, London, Special Publications, 141, 1-14.

Worsley, D., (2008). *The post-Caledonian development of Svalbard and the western Barents Sea.* Polar research, Volume 27, pp. 298-317.

Ziegler, P. A., (1988). *Evolution of the arctic-north atlantic and the western tethys - A visual presentation of a series of paleogeographic-paleotectonic maps.* Search and Discovery Article #30002

Webpages

NPD. (1985). Norwegian Petroleum Directorate Factpages [Online]. Retrived 16.03.2017 http://factpages.npd.no/ReportServer?/FactPages/PageView/wellbore_exploration&rs:Command=Render&rc:Toolbar=false&rc:Parameters=f&NpdId=473&IpAddress=129.242.205.24&CultureCode=nb-no

NPD. (1986). Norwegian Petroleum Directorate Factpages [Online]. Retrived 16.03.2017 http://factpages.npd.no/ReportServer?/FactPages/PageView/wellbore_exploration&rs:Command=Render&rc:Toolbar=false&rc:Parameters=f&NpdId=896&IpAddress=129.242.205.34&CultureCode=nb-no

NPD. (1987). Norwegian Petroleum Directorate Factpages [Online]. Retrived 16.03.2017 http://factpages.npd.no/ReportServer?/FactPages/PageView/wellbore_exploration&rs:Command=Render&rc:Toolbar=false&rc:Parameters=f&NpdId=1066&IpAddress=129.242.205.34&CultureCode=nb-no

NPD. (2004). Norwegian Petroleum Directorate [Online]. Retrived 18.03.2017 http://www.npd.no/en/news/News/2004/Cold-opportunities-/

NPD. (2005). Norwegian Petroleum Directorate Factpages [Online]. Retrived 16.03.2017 http://factpages.npd.no/ReportServer?/FactPages/PageView/wellbore_exploration&rs:Command=Render&rc:Toolbar=false&rc:Parameters=f&NpdId=5039&IpAddress=129.242.205.24&CultureCode=nb-no

NPD. (2017a). Norwegian Petroleum Directorate [Online]. Retrived 09.03.2017 http://www.npd.no/en/Topics/Geology/Geological-plays/

NPD (2017b). Norwegian Petroleum Directorate Factpages [Online]. Retrived 01.12.2017 http://factpages.npd.no/ReportServer?/FactPages/PageView/strat_Litho_level1_group_formation&rs:Command=Render&rc:Toolbar=false&rc:Parameters=f&NpdId=138&IpAddress=129.242.205.51&CultureCode=en

NPD (2017c). Norwegian Petroleum Directorate Factpages [Online]. Retrived 18.03.2017 http://factpages.npd.no/ReportServer?/FactPages/PageView/field&rs:Command=Render&rc:Toolbar=false&rc:Parameters=f&NpdId=2053062&IpAddress=129.242.206.180&CultureCode=nb-no

NPD (2017d). Norwegian Petroleum Directorate [Online]. Retrived 25.04.2017 http://www.npd.no/en/news/News/2017/Doubling-the-resource-estimate-for-the-Barents-Sea/